Multimodal and multisensory coding in the *Drosophila* larval peripheral gustatory center

G. Larisa Maier[1], Marjan Biočanin[2], Johannes Bues[2], Felix Meyenhofer[1], Clarisse Brunet Avalos[1], Jae Young Kwon[3, 4], Bart Deplancke[2, 4] and Simon G. Sprecher[1,4,5]

[1]Department of Biology, University of Fribourg, 1700 Fribourg, Switzerland

[2]Laboratory of Systems Biology and Genetics, Institute of Bioengineering, School of Life Sciences, EPFL and Swiss Institute of Bioinformatics (SIB), 1015 Lausanne, Switzerland

[3] Department of Biological Sciences, Sungkyunkwan University, Suwon 16419, Republic of Korea

[4] J.Y.K., B.D. and S.G.S. are co-senior authors.

[5] To whom correspondence should be addressed. Email: simon.sprecher@unifr.ch

Abstract

The ability to evaluate food palatability is innate in all animals, ensuring their survival. The external taste organ in *Drosophila* larvae is composed of only few sensory neurons but enables discrimination between a wide range of chemicals and displays high complexity in receptor gene expression and physiological response profile. It remains largely unknown how the discrepancy between a small neuronal number and the perception of a large sensory space is genetically and physiologically resolved. We tackled dissection of taste sensory coding at organ level with cellular resolution in the fruit fly larva by combining whole-organ calcium imaging and single-cell transcriptomics to map physiological properties and molecular features of individual neurons. About one third of gustatory sense neurons responded to multiple tastants, showing a rather large degree of multimodality within the taste organ. Further supporting the notion of signal integration at the periphery, we observed neuronal deactivation events within simultaneous neighboring responses, suggesting inter-cellular communication through electrical coupling and thus providing an additional level in how neurons may encode taste sensing. Interestingly, we identified neurons responding to both mechanical and taste stimulation, indicating potential multisensory integration. On a molecular level, chemosensory cells show heterogeneity in neuromodulator expression. In addition to a broad cholinergic profile, markers on dopaminergic, glutamatergic or neuropeptidergic pathways are present either in distinct cell populations or are seemingly co-expressed. Our data further extend the sensory capacity of the larval taste system pointing towards an unanticipated degree of multimodal and multisensory coding principles.

Introduction

Taste sensing provides the innate ability in all animals to avoid toxic or deleterious food ingestion and to choose a nutritious diet. The fruit fly larva is able to discriminate between a large range of different gustatory cues (1), being – similarly to humans – repelled by bitter tastants (2-4) as possible signals of toxic food, and attracted by sweet and certain amino acids (5-7), indicators of a nutritious diet. Distinct from mammals where hundreds of taste cells are assembled in taste buds on the tongue, the larva disposes of very few gustatory sense neurons (GSNs) at the periphery (8, 9), raising the question of how does a small neuronal population encode a large palette of cues.

Distinct models of sensory coding have emerged for taste perception. According to the labeled-line model, each cell within a mammalian taste bud is tuned to one of the 5 basic tastes – sweet, umami, bitter, sour and salt (10-13). This model relies to a large extent on the existence of a best stimulus concentration (14) but varying the concentration of a given tastant alters the number of responding cells and afferent sensory neurons, often increasing the proportion of multituned neurons (15). Moreover, taste cells within a bud have been shown to communicate with each other through purinergic signaling (16), entailing coexistence of narrowly and broadly tuned taste sensing cells (17) and signal integration at the periphery, distinct from a strictly segregated taste sensing model.

In *Drosophila* taste sensing has been described in accordance with a labeled-line model, as sweet, bitter and water perception localize in separate populations of peripheral GSNs (18-22). However, additional tastes such as salt, fatty acid, carbonation, polyamines or amino acids partially overlap onto sweet or bitter sensing GSNs by means of specific added-on

receptor expression (23-30), suggesting a model of taste sensing with both narrowly and more broadly tuned cells, similar to mammals.

The peripheral gustatory system in the *Drosophila* larva presents many similarities with the adult fly, such as the sensillar organization of dendrites, presence of both internal and external chemosensory organs (31), as well as cue detection through the same chemoreceptor gene families – GRs (Gustatory Receptors), IR (Ionotropic Receptors), PPKs (pickpocket) or TRPs (Transient Receptor Potential) (29, 32-38). On the other hand, larval taste processing presents developmental stage particularities, considering that the number of GSNs is much lower than in adult flies and many receptors are larva-specific (39, 40).

The main chemosensory organs in *Drosophila* larva are located at the tip of the head, represented by ganglia of bipolar sensory neurons (Fig.1A) (41). External organs include the terminal organ ganglion (TOG) – with main taste, but also mechano- and thermo-sensory function, the dorsal organ ganglion (DOG) – with primary olfactory role, and the smaller, generally uncharacterized ventral organ ganglion (VOG) – with associated taste function (8). Sensory neurons in these ganglia extend dendrites to the periphery in direct contact with the environment and axonal projections into defined regions of the brain. Conversely, internal chemosensory organs called ventral, dorsal and respectively posterior pharyngeal sensories (VPS, DPS, PPS) are located on the pharyngeal tube where they project their dendrites (42), therefore functionally associated with taste sensing during food ingestion.

Thanks to the 1 to 1 receptor to neuron expression in the DOG, functional dissection of the 21 olfactory sensory neurons was achieved using corresponding Gal4 lines (43-47). In contrast, the neighboring TOG, main external larval taste center, comprises more than 30 GSNs out of which only 7 neuronal identities (C1-C7) have been mapped and can be traced using individual Gal4 lines (Fig.1B) (39, 48, 49). Characterization of single larval GSNs has

86 revealed multimodality and even taste integration of opposed valence within one GSN (48),
87 but the general taste sensing logic in this animal remains largely unexplored.

88 We here delve into sensory tuning diversity of TOG neurons by using whole-organ in-vivo
89 calcium imaging recordings on larvae expressing genetically encoded calcium sensors. To
90 gain insight into molecular components of TOG and DOG neurons we employed DisCo, a
91 novel approach that enables single-cell RNA sequencing of low input samples (50). Our
92 findings provide insights into fundamental aspects of taste sensory coding. First, we show that
93 roughly one third of responding GSNs are activated by more than one taste modality, while
94 conversely, single tastants generally elicit responses in several neurons. Interestingly, we
95 detected neuronal deactivation responses, distinct from canonical calcium imaging signals,
96 which occurred within concomitant firing in adjacent neurons, as described for electrical
97 coupling in the adult fly olfactory system (51, 52). Using DisCo and immunostainings, we
98 identified distinct and common molecular markers in TOG/DOG neurons. While it was
99 known that larval chemosensory neurons are cholinergic (53), we found that they are also
100 glutamatergic and dopaminergic, and, similar to the central nervous system (CNS) (54),
101 neurons may also co-express neurotransmitter markers. Lastly, we detected expression of
102 mechanosensory receptor genes and, intriguingly, GCAMP recordings showed activation to
103 both mechanical and chemical stimulation in some neurons, implying multisensory
104 integration at single cell level. Taken together, our observations of the larval external
105 gustatory organ bring evidence of multimodality, possibly inter-cellular communication
106 through electric coupling, heterogeneous expression of neurotransmitter markers and
107 mechanosensory features in GSNs.

Results

Whole organ larval taste recordings with single cell resolution

Due to the sparse availability of Gal4 lines for individual GSN labeling in the larva, assessing an overview of peripheral taste coding by tackling single neurons entails limitations. We therefore undertook characterization of TOG neurons by means of a whole-organ approach.

First, we performed immunostainings on individual GSNs expressing *myr*:*GFP* (Fig.1C & D). Structural flexibility of this tissue entails variability across samples but we noted the 7 previously identified GSNs maintained a relatively stereotypical localization between stainings (n≥3) (Fig1C). This allowed assembling 3D locations of the 7 GSNs, serving as approximation map of their respective position within the organ (Fig.1D).

Further, we performed whole-organ calcium imaging recordings by expressing cytoplasmic GCaMP6m (55) and nuclear RFP (56) reporters in all neurons driven by *nSyb*-Gal4 (Fig.1E). The use of a nuclear reporter as cellular landmark was critical for whole organ recordings, as solely a cytoplasmic fluorophore would not sufficient for efficient segmentation due to low baseline fluorescence intensity in some cells and to ambiguous delimitation between neighboring somata. As previously described (57), we made use of a customized microfluidic chamber for chemical stimulation while recording physiological responses of all GSNs in a semi-intact larval preparation, and we subsequently developed a data processing pipeline for whole organ recordings (Suppl.Fig.1).

One third of responding GSNs show taste multimodality

We first tested two distinct series of chemicals each containing 5 substances belonging to the 5 canonical taste categories: sweet, bitter, sour, amino acids and salt. Substances and concentrations were chosen according to former studies (48, 58) (Table1, Fig.2A, see Methods). Out of all responding neurons across 15 total recorded organs, 66% showed activation to only one tastant per animal and most unimodal responses were recorded to sucrose and high salt (Fig.2A, uni-taste/cell). In line with our previous findings that some GSNs are multimodal (48), the remaining 34% of responding neurons were activated by more than one substance (Fig.2A, Suppl.File1), showing that several larval GSNs have the capacity to respond to different taste categories. The top 5 taste response combinations mapping to one neuron (Fig.2A, multi-taste/cell) were: sucrose and valine/arginine (sweet + amino acid, 17%), sucrose and citric acid (sweet + sour, 17%), citric acid and high salt (sour + high salt, 14%), sucrose and high salt (sweet + high salt, 14%) and finally sucrose and denatonium/quinine (sweet + bitter, 14%). Interestingly, sucrose was the tastant corresponding to most uni-taste/cell responses but also to most frequent taste combinations of multi-taste/cell.

Next, we expanded the number of gustatory cues used for GSN stimulation by using groups of tastants for sweet, bitter, amino acid and salt taste categories (Fig.2B, Suppl.Table 1). To begin with, we tested 2 groups of sugars, chosen as monosaccharides (fructose, glucose, arabinose, mannose, galactose), and respectively disaccharides (sucrose, trehalose, maltose, lactose, cellobiose). We calculated a rounded 74% of sugar-responsive neurons to be activated by either monosaccharides (41%) or disaccharides (33%), and a rounded 25% by both groups (Fig.2B, upper left panel).

For salt taste stimulation we mixed NaCl and KCl for a final concentration of 50mM for low salt group and respectively 1M for high salt group. We observed a low percentage of cell

activation overlap among salt-responding cells, 20% being activated by both groups while the rest responded either to high salt (56%) or to low salt (24%).

The 20 proteinogenic amino acids were compiled in 4 groups (A, B, C and D) as previously described by Park et al. (59) (Suppl.Table 1). 38% amino acid-responding neurons showed activation to 2 or more amino acid groups. Similar percentages were observed for animals stimulated with all 8 groups (2 sugar, 2 salt and 4 amino acid units), with up to 40% neurons responding to at least 2 different taste modality groups (Fig.2B upper right panel).

Bitter tastants were randomized in 2 groups of 4 substances each (Suppl.Table 1): DSoTC group (denatonium benzoate, sucrose octaacetate, theophylline, coumarin), and respectively QLSC group (quinine, lobeline, strychnine, caffeine). Among cells responsive to bitter stimulation we observed a bigger fraction of cells activated by DSoTC group (55%) than by QLSC (30%). In animals tested for sweet and bitter taste response, the percentage of cells activated by both sugar and bitter groups was of 30% (Fig.2B, lower panels), in agreement with cell integration of tastants with opposite valence.

Taste stimulation can elicit either activation or deactivation signals in GSNs

While canonical responses of GSNs to taste cues entail a rise of GCaMP fluorescence, we also detected neuronal responses characterized by a fluorescence intensity decrease. For simplicity, and not as conclusive categorization, we named these observed intensity fluorescence decrease signals: *deactivation responses*, as they are seemingly opposite to canonical neuronal activation measured through fluorescence increase.

A notable example of deactivation was recorded in response to citric acid in 2 neurons localized centrally in the organ in close proximity with each other. We termed these neurons

178 CDL1 (central-dorsal-lateral neuron 1) and CDL2, respectively. Intriguingly, CDL1 and
179 CDL2 responded to citric acid in a pattern of synchronous activation-deactivation (Fig.3A).

180 To examine into the possibility that deactivation responses were caused by top-down
181 inhibition by central interneurons, we performed recordings in animals with severed
182 connections between chemosensory neurons and CNS (Fig.3B). Detaching the brain and the
183 respective sensory nerve connections did not abolish the activation-deactivation responses
184 induced by citric acid stimulation. Likely, this pattern corresponds to ephaptic transmission
185 where the electrical field of a responding cell generates hyperpolarization in the partner cell
186 (60), also reported in the adult olfactory system (51).

187

188 **Mapping neuronal responses across larvae shows a high level of taste multimodality**
189 Next, we proceeded to match neurons based on their spatial position within the TOG organ
190 and responses recorded to individual taste series presented in figure 2A. We identified and
191 named 21 GSNs (Fig.4, y axis and 3D image). All considered responses exceeded 20% DF/F0
192 and were manually validated. Not all neurons showed the same response consistency, as
193 reflected by the stereotypy of response, meaning the percentage of times a neuron was
194 identified to respond (Fig.4A freq, grey tones with darker color denoting higher frequency).
195 Heatmap for activation and deactivation responses for each neuron were compiled separately
196 and for each cell and each tastant, we plotted the stereotypy of response next to the average
197 intensity of response (Fig.4A, x axis). Average intensities were considered only if response
198 frequencies were at least 20% for the given tastant.

199 Although deactivation responses were noted to different substances in different neurons
200 (Fig.4A, blue ovals), such events with frequency of response above 20% were only mapped to
201 CDL2 and CPV neurons, particularly for citric acid stimulation. Noteworthy, CDL1 was

202 robustly activated by citric acid while its CDL2 neighbor showed robust deactivation in
203 response to citric acid (Suppl.File2, Wilcoxon signed rank nonparametric test, $p<0.05$)
204 (Fig.4C), as described for their concomitant response pattern in figure 3.

205 While most GSN identities cannot be pinned down with absolute certainty, we identified the
206 AC1 neuron to likely share identity with the previously described C6 neuron, based on the
207 easily recognizable anterior position in the organ (Fig.1C & 4B) and response profiles to
208 sucrose and high salt as previously reported for C6 (48) (Fig.4D).

209 Taken together, the physiological results show an important degree of taste integration and
210 complexity – a tastant can elicit responses from multiple GSNs and a GSN can respond to
211 multiple tastants per animal or across animals, suggesting a combinatorial mode of sensory
212 encoding.

213

214 **Molecular profiles of TOG and DOG neurons at single cell resolution**

215

216 In order to assess molecular features of individual sense neurons we performed single cell
217 transcriptomic experiments on the TOG and the DOG. Due to low neuronal number and to
218 restricted access to the tissue, the choice of methodology was a limiting and important factor.
219 To generate single cells in suspension at the level of sense organs we proceeded with their
220 isolation by manual picking (Fig.5A) and importantly, we employed a deterministic DropSeq
221 approach for low cell numbers (50, 61), resulting in increased efficiency of encapsulation
222 compared to classical approaches (62, 63).

223 The single cell data was analyzed in Seurat v3.1.2 (64, 65) (Suppl.Fig.5B, see Methods),
224 obtaining a dataset of 153 cells with more than 400 genes per cell. We used UMAP

225 embedding for visualization of marker gene expression (Suppl.Fig5C) and confirmed
226 neuronal identity of the relatively homogenous cell population based on neuronal gene
227 markers (Fig.5B). Moreover, we could detect distinct and non-overlapping expression of
228 marker genes for gustatory and olfactory sensory cells. Specifically, the *Orco* gene (*Odorant*
229 *receptor co-receptor*) that is present in all olfactory neurons in the DOG (43), most probably
230 labels the olfactory neuronal population. Conversely, *proboscipedia (pb)*, a gene known to
231 mediate specification of adult mouthparts (66), shows no overlap of expression with *Orco*-
232 positive cells, labeling a distinct neuronal population (Fig.5C, left). Importantly,
233 immunofluorescence staining in embryos shows *pb* expression restricted to TOG neurons and
234 non-overlapping with *Orco* (Fig.5C, right). Furthermore, expression of the two marker genes
235 largely correlated with the two generated clusters, although less defined for *Orco*, which
236 shows a more dispersed cell expression pattern (Suppl.Fig5C).

237

238 **Chemosensory neurons display broad and narrow expression of neurotransmitter**
239 **markers**

240 To further explore molecular neurotransmitter profiles of sense neurons we performed
241 immunostainings of marker genes on distinct neuromodulator pathways. Using *Cha*-Gal4
242 (67), we found *Choline acetyltransferase (ChAT/Cha*) in virtually all sense neurons in
243 imunofluorescence staining (Fig.6A, left), corresponding to a relatively broad molecular
244 expression (Fig.6A, right). Conversely, we identified *pale (ple)* as being expressed in 2 cells
245 of the TOG as shown by TH antibody staining (Fig.6B, left), and corresponding to a cell
246 group identified in the UMAP embedding colored by expression (Fig.6B, right). *Pale* encodes
247 a tyrosine hydroxylase as the first step on dopamine synthesis pathway and is orthologous to
248 human *tyrosine hydroxylase (TH).*

Other neurotransmitter markers have also shown selective molecular expression, as in the case of *Vesicular glutamate transporter* (*VGlut)*. Immunofluorescence on *VGlut*-Gal4 larvae exposes three cells – one in the TOG, one in the DOG and a third cell in a group peripheral to TOG, we named here Mec (Fig.6C). We verified the response profile of these neurons by recording their physiological response to tastants introduced earlier (Fig.2A), and we compared the response for each tastant with the water response. We noted sucrose responses to be different than control in the TOG and the DOG neurons (Fig.6D, Suppl.File3, $p<0.05$, Mann-Whitney test), whereas Mec cell didn't show responses distinct from water to any of the tested substances. The TOG *VGlut*-positive cell did not show co-expression with C7, C2 or C1-Gal4 (Suppl.Fig6), its identity remaining to be determined.

We have detected co-expression of markers on shared neuromodulatory pathway, as in the case of *Dopamine transporter (DAT)* and *Vesicular monoamine transporter (Vmat)* (Fig.7A). Considering that *Cha* is expressed in all chemosensory neurons according to immunofluorescence observations (Fig.6A), co-expression could be theoretically deduced between this and any other neurotransmitter revealed by the molecular data. Specifically, we have detected *Cha* and *DAT* co-localization in a small subset of cells as illustrated in Fig.7B. Additionally, we have identified several neurotransmitter receptors linked to GABA, serotonin, octopamine or dopamine signaling pathways, some of them showing co-expression in certain neurons, as for example *GABA-B-R2* and the serotonergic receptor *5-HT2B* (Fig.7C). Moreover, neuropeptide expression was also abundant in our data, such as neuropeptide-like 2/4 precursors (*Nplp2, Nplp4*), also co-expressed with other neurotransmitter markers such as *VGlut* or *Vmat* (Fig.7D & E). Co-expression of several neuromodulators in numerically restricted neuronal tissues such as the TOG and DOG supports the multimodal character of these sense organs but the functional implication of this observation remains an open question.

GSNs show mechanosensory marker expression and responses

Mechanosensory function in the larval taste sensing was assumed to a large extent due to early microscopic descriptions of chemosensory organs in *Drosophila* and in other insects (9, 68, 69). Although functional investigations of mechanical and chemosensory integration have been explored in the adult fly (70, 71), similar studies in the larva were primarily focused on food texture effects in taste behavior and learning (72, 73) while the involved mechanoreceptors remain unknown. We identified expression of mechanosensory markers both by means of immunofluorescence stainings and in single cell UMAP embedding (Fig.8). Namely, *nanchung* (*nan*) is expressed in one TOG and one DOG cell (Fig.8A), whereas *no mechanoreceptor potential C* (*nompC)* is present in a group of 3-4 cells of the TOG and surrounding smaller sensilla (Fig.8B). We found expression of *painless* (*pain*-Gal4) by means of immunolabelling in a population of up to 12 TOG cells, corresponding to a few single cells in the UMAP embedding. Knowing that *pain* is involved in mechanical and thermal nociception in multidendritic and chordotonal sensory neurons in the larva (74), we further tested the response profiles in *pain*-expressing TOG neurons to mechanical stimulation (Fig.8C).

To measure mechanical responses we aimed at inducing fluid shear stress on the cellular membrane (75) and measuring the cell response after turning on the water flow inside the microfluidic chip. As the tissue was exposed to water also during the off stimulus (in absence of flow), we interpreted neuronal responses to be determined by the fluid flow and not by water taste itself. We detected fluorescence intensity changes on average in 4 *pain*-Gal4 cells, which were named based on their relative position and mapped to the organ. More often than

297 not, although not exclusively, we observed fluorescence intensity decrease during the on
298 stimulus, *pain*-expressing cells being potentially de-activated by shear stress (Fig.8C).

299 In a separate assay we recorded *nsyb*-Gal4 larvae for mechanosensory as well as taste sensing.
300 Interestingly, in few cases we observed neurons activated by both types of modalities, as for
301 example CM1 neuron responding to 500mM sucrose but also showing de-activation to
302 mechanical shear stress (Suppl.Fig8). This observation suggests that some GSNs could
303 integrate both mechano- and taste sensing as previously suggested (8).

304

Discussion

In this study we explored the physiological and molecular characteristics of *Drosophila* larval taste system. We designed an experimental framework allowing calcium imaging in all GSNs comprised by the larval primary taste-sensing organ at the periphery (the TOG, Fig.1, Suppl.Fig.1). Our approach complements previous strategies based on labeling of few single neurons or subpopulations (6, 29, 35, 39, 48), allowing for an overview of activation patterns within the organ. Strengthening our previous observations on the multimodal character of larval taste neurons (48), we identified single GSNs activated by different taste categories as well as single GSNs activated by tastants with opposite associated valence. Cell integration of different tastes might involve spatio-temporal codes, as described for gustatory discrimination in the moth (76) or combined patterns of response in cell number and type of activation. In line with our observations that one tastant elicits response in several GSNs, it is interesting to consider that the relevance of a stimulus and ultimately its behavioral output could depend on neurons firing together, concurrent activation of 2 neurons differing from their separate activation (77).

For the substances tested within this study we observed roughly a 60-70% versus 30-40% division of uni-modal versus multi-modal responding GSNs (Fig.2 & 4), comparable with tuning proportions reported for mouse fungiform taste sensing cells (78). The *best stimulus concentration* principle is arguably the strongest support of the labeled-line taste coding at the periphery in the mammalian system (79). However, this model leaves out the case of tastants activating different types of taste receptors depending on concentration as in the case of acesulfame K and saccharin, which at low concentrations activate sweet receptors but with increased concentration start activating bitter receptors (12). Accordingly, the chosen

329 substance concentrations within our assay might cause variability in response profiles, and
330 doubtlessly, modifying the dilution for the same tastants would alter the observed tuning of
331 GSNs, as shown on afferent taste neurons in mammals (15).

332 An intriguing aspect of taste physiology revealed by our observations was GCaMP
333 fluorescence decrease in GSNs, termed here *deactivation* for ease of discussion. Most notable
334 deactivation signals were recorded in CDL2 neuron and most stereotypically to citric acid
335 (Fig.3 & 4), although the phenomenon was not restricted to this neuron or tastant.
336 Interestingly, citric acid elicited concomitant activation in the neighboring cell named CDL1,
337 indicating response patterns of activation-deactivation in the CDL1-CDL2 couple, similar to
338 ephaptic signaling identified in the olfactory system of the adult fly (51). The synchronous
339 responses were not abolished when severing afferent neuronal axons (Fig.3B), implying that
340 CDL2 deactivation is not determined by a top-down inhibition from brain interneurons.
341 Additional possible explanations of the observed neuronal activity include gap junction
342 communication or tonic activity in CDL2 inhibited by citric acid stimulation, as reported in
343 sensory neurons of bumblebees and respectively in *C.elegans* (81, 82). However, the observed
344 synchronous activation coupled with deactivation responses in adjacent neurons best fit the
345 description of ephaptic signaling (60, 80), pointing towards inter-cellular communication and
346 thus emphasizing a model of signal integration in larval taste system at the periphery.

347

348 Using DisCo allowed us to successfully probe larval chemosensory organs with single cell
349 resolution (Fig.5, Suppl.Fig.5), resolving low cell input and tissue accessibility limitations.
350 We identified *pb* and *Orco* as marker genes distinctly expressed in TOG and respectively in
351 DOG neurons. If *Orco* is an olfactory co-receptor expressed in all olfactory neurons, taste

neuronal population is less characterized and functionally more diverse. Therefore, *pb* could be an interesting candidate for further characterizing the population of *pb*-expressing GSNs.

Moreover, in the present work we describe distinct expression patterns of neuromodulator marker genes in TOG and DOG neurons, as shown by UMAP embedding and confirmed by immunostainings (Fig.6). The cholinergic profile of larval chemosensory neurons has previously been reported (31, 53) but we show that some cells express glutamatergic, dopaminergic and neuropeptidergic markers. Interestingly, marker genes on different signaling pathways are co-expressed in subsets of cells (Fig.7), as previously demonstrated in *Drosophila* CNS (54, 83). Considering the multimodal character of some larval GSNs, it would be fascinating to uncover the role played by co-expression of distinct neurotransmitter markers in such neurons. Nevertheless, if remains surprising that a handful of sensory neurons display a diverse neurotransmitter profile, as reported here, demonstrating a large molecular diversity within the neuronal sensory population.

Furthermore, we found expression of mechanosensory markers as revealed by UMAP embedding of single-cell data and verified with immunostainings. We detected *nan* in one TOG neuron and one DOG neuron, whereas *nompC* and *pain* label a larger population. We recorded responses of *pain*–expressing GSNs exposed to water flow turned on and off, as we intended to create fluid shear stress on the cell membrane, similarly to observations on cultured cells (84) and studies on vascular tissue (85). It remains to be elucidated if shear stress responses detected in *pain* neurons are mediated by Painless channel itself. Painless is a protein known to be important in mechanical and thermal nociception in larvae (74), although its role remains unexplored in the gustatory system. On the other hand, Painless has also been shown to be involved in wasabi taste detection in adult flies in Gr66a-expressing GSNs (86) and we have also found scarce co-expression between *pain* and *Gr66a* (data not shown). The presence of mechanosensory neurons in the larval primary taste center has been frequently

reported (9, 49). Although chemosensory sensilla have been classically described as distinct from mechanosensory sensilla (87), existence of neurons with dual chemo- and mechanosensory modalities has also been implied based on their tubular dendritic body (8). In our observations, some mechano-responsive neurons also show activation to gustatory cues (Suppl.Fig.8), stressing on the probability of multisensory integration of taste and mechanical cues.

Taken together, our data suggest a complex taste sensory coding in the larva, made up by patterns of activity across neurons rather than by labeled individual neuronal responses for discrimination between tastants. Besides canonical fluorescence increase responses we have depicted fluorescence decrease signals in specific neurons pointing towards electric coupling and therefore sensory cue processing at the periphery. Additionally, the neurotransmitter and mechanoreceptor expression contribute to the multifaceted chemosensory system to potentially explain the multimodality and multisensory character of specific taste neurons in future studies.

Methods

Fly stocks.

We used the following fly strains: *nSyb*-Gal4 (gift from Shanhaz Lone), UAS-*GCaMP6m* (Bloomington #42748), UAS-*H2B:RFP* (gift from Boris Egger), *GMR57BO4*-Gal4 (Bl. #46355), *Gr94a*-gal4 (Bl. #57686), *Gr21a*-Gal4 (Bl. #23890), *Gr22e*-Gal4 (Bl. #57608), *Gr66a*-Gal4 (Bl. #57670), *Gr97a*-Gal4 (Bl. #57687), *Gr59e*-Gal4 (Bl. #57655), UAS:*mcd8:GFP;Or83b:RFP* (gift from Travis Carney), UAS-*myr:GFP* (Bl. #32198), *VGlut*-Gal4 (Bl. #24635) , *VGAT*-Gal4 (Bl. #58980), *Cha*-Gal4 (kindly gifted by PM Salvaterra), *nan*-Gal4 (Bl. #24903), *nompC*-Gal4 (Bl. #36361), *pain*-Gal4 (Bl. #27894), FlyFos *Orco*-GFP (VDRC 318654).

Immunostainings.

3rd instar larvae (4 days after egg laying) were washed and dissected in ice-cold PBS. Tissue containing chemosensory neurons was fixed in 3,7% formaldehyde for 18-20min at room temperature. After fixation, incubation in primary antibodies was performed at 4°C overnight, then in secondary antibodies at 4°C overnight, and finally, in Vectashield antifade medium (Vector Laboratories) for at least 1h before mounting the samples on microscope slides. After each step described above, PBST (PBS 0,3% Triton X-100) was employed for three consecutive plus three 30-minute washes at room temperature.

Immunolabelling against Pb (Fig.5C) was performed at embryonic stage. Embryos were washed in tap water and placed in a plastic mesh in a sampling manifold. (Millipore XX2702550). First, they were dechorionated in 2.5% sodium hypochlorite (household bleach)

414 for 2 minutes. Embryos were then fixed in a 1:1 solution of n-heptane:PEM buffer with 3.7%
415 formaldehyde for 20 minutes at room temperature on a rotating wheel. Upon fixation,
416 embryos were washed with methanol and blocked for 1 hour at room temperature with 5%
417 normal goat serum in PBST. The samples were incubated with antibodies and mounted as
418 described above.

419 Confocal images were acquired on a Leica TCS SPE-5 confocal, using the 40x oil immersion
420 objective for larval staining and the 63X glycerol immersion for embryo staining, at 0.8-1um
421 slice thickness. Images were assembled using Fiji (88) and Adobe Illustrator.

422 Primary antibodies: chicken anti-GFP (1:1000, Abcam, ab13970), rabbit anti-DsRed (1:1000,
423 Clontech, No. 632496), rat anti-ELAV (1:30, No. 7E8A10), anti-TH (1:100, Millipore,
424 ab_390204), rabbit anti-Pb 1:100 (gift of Thomas Kaufman, Cribbs, 1992 #475). Secondary
425 antibodies conjugated with Alexa Fluor fluorescent proteins (488, 568, 647) were used in
426 dilution of 1:200 (Molecular Probes no. A-11008, A-11039, A-21244, A-21247, A-11011).

427

428 **Chemicals**.

429 For calcium imaging experiments the highest purity available was chosen for all chemicals
430 used in this study: L-Alanine (Sigma-Aldrich, 56-41-7), L-Glutamine (Sigma-Aldrich, 56-85-
431 9), L-Aspartic acid (Sigma-Aldrich, 56-84-8), L-Glutamic acid (Sigma-Aldrich, 56-86-0), L-
432 Asparagine (Sigma-Aldrich, 70-47-3), L-Proline (Sigma-Aldrich, 147-85-3), L-Tyrosine
433 (Sigma-Aldrich, 60-17-4), L-Threonine (Sigma-Aldrich, 72-19-5), L-Phenylalanine (Sigma-
434 Aldrich, 63-91-2), L-Lysine (Sigma-Aldrich, 56-87-1), L-Arginine (Sigma-Aldrich, 74-79-3),
435 L-Histidine (Sigma-Aldrich, 71-00-1), L-Serine (Sigma-Aldrich, 56-45-1), L-Valine (Sigma-
436 Aldrich, 72-18-4), L-Cysteine (Sigma-Aldrich, 52-90-4), L-Methionine (Sigma-Aldrich, 63-

68-3), L-Leucine (Sigma-Aldrich, 61-90-5), L-Isoleucine (Sigma-Aldrich, 73-32-5), L-Tryptophan (Sigma-Aldrich, 73-22-3), L-Glycine (Roth, 3187.3), D-Sucrose (Sigma-Aldrich, 57-50-1), D-Glucose (Sigma-Aldrich, 50-99-7), G-Fructose (Fluka, 57-48-7), D-Trehalose dihydrate (Roth, 9286.1), D-Arabinose (Sigma-Aldrich, 10323-20-3), D-Maltose monohydrate (Sigma-Aldrich, 6363-53-7), D-Mannose (Sigma-Aldrich, 3458-28-4), D-Galactose (Roth, 4979.1), D-Cellobiose (Roth, 6840.3), Lactose monohydrate (Roth, 8921.1), Quinine hemisulfate salt monohydrate (Sigma-Aldrich, 6119-70-6), Denatonium benzoate (Aldrich, 3734-33-6), Caffeine anhydrous (Fluka, 58-08-2), Coumarin (Sigma-Aldrich, 91-64-5), Sucrose octaacetate (Aldrich, 126-17-7), Lobeline hydrochloride (Aldrich, 134-63-4), Theophyline (Sigma-Aldrich, 58-55-9), Strychnine (Roth, 4843.1), Potassium chloride (Merck, 7447-40-7), Sodium chloride (Sigma-Aldrich, 7647-14-5), Citric acid (Sigma-Aldrich, 77-92-9).

Chemicals used in cell dissociation experiments: elastase (Sigma-Aldrich, E0258), collagenase (Sigma-Aldrich, C9722), PBS (Thermo Fisher Scientific, AM9624), BSA (Thermo Fisher Scientific, AM2616), Murine inhibitor (New England Biolabs (NEB, M0314L).

Calcium imaging.

The semi-intact sample for calcium-imaging recordings was prepared as previously described (57). 3rd instar larval heads comprising chemosensory neurons, the brain and the connecting nerves were dissected in AHL (adult hemolymph like) saline solution. The tissue was introduced into the microfluidic chip and the sample was connected to the tubing and micropump setup. For whole organ TOG recordings UAS-*GCaMP6m* (55) was used to genetically label all neurons and *RFP* was expressed in nuclei using UAS-*H2B:RFP* (56).

Stacks were set to 15 slices of 1,5 µm thickness each, pixel binning of 2, with resulting time acquisition speed of 0.5 stacks (time-points) per second. For recordings from *VGlut*-Gal4 neurons, we used the same UAS reporter lines to image the three neurons belonging to the TOG and the DOG, but due to a deeper tissue extending over both organs, we set the stacks to 25 slices of 2,5 µm thickness each, preserving the time acquisition speed.

The microscope of choice was a spinning-disk confocal Visitron CSU-W1. Recordings were exported as .nd files and further processed in Fiji/ImageJ and Imaris software. For each recording an RFP stack was acquired prior to the CGaMP time-series.

Taste Stimulation. Each tastant was administered using a micropump (mp6, Bartels Mikrotechnik) controlled in VisiView software through built-in macros. Millipore water was used as solvent for taste solutions and as washing control. For each taste stimulation macros were designed for 2-minute recordings to allow 1 minute pre-wash followed by 30-second stimulation and a final 30-second wash.

Taste stimulation with series of individual tastants. The sequence of chemicals within a trial was randomized. We used two series of tastants (Suppl.Table 1), each containing 5 substances from 5 different taste categories. Series 1 consisted of sucrose (sweet), denatonium (bitter), NaCl 1M (high salt), valine (amino acid) and citric acid (sour). Series 2 consisted of sucrose, quinine (bitter), NaCl 100mM (low salt), arginine (amino acid) and citric acid. Each recorded animal was stimulated with all the tastants within one series. A total of 15 TOG organs were recorded, 7 for series 1 and 8 for series 2.

Taste stimulation with groups of tastants. We compiled 2 groups of sugars, each containing 5 sugars at a concentration of 100 mM each: monosaccharides (fructose, glucose, arabinose, mannose, galactose), and disaccharides (sucrose, trehalose, maltose, lactose, cellobiose). Amino acids were prepared in 4 groups (A, B, C and D) as previously described by Park et al.

485 (59) (Suppl.Table 1). Tyrosine was included in group B at a concentration of 1mM. Salt taste
486 groups contained NaCl and KCl in equal proportions at a total concentration of 50mM (low
487 salt) and respectively 1M (high salt). Bitter tastants were randomized in 2 groups of 4
488 substances each, with a final concentration of 22mM and respectively 13mM, restricted by the
489 solubility of certain substances such as lobeline or strychnine reduced to 1mM instead of
490 10mM (Suppl.Table 1): DSoTC group (denatonium benzoate, sucrose octaacetate,
491 theophylline, coumarin), and respectively QLSC group (quinine, lobeline, strychnine,
492 caffeine).

493 **Mechanical stimulation.** Macros were adjusted to switch water flow between on and off at
494 30-second interval. The sample was exposed to water in both conditions; therefore,
495 corresponding neuronal responses were interpreted to be result of shear stress mechanical
496 stimulation (75) and not caused by water taste.

497

498 **Data processing and analysis of whole-organ physiological recordings.**

499 We first carried out deconvolution processing on Huygens platform of RFP stacks and
500 GCaMP recordings. A Fiji/ImageJ plugin was written to duplicate the RFP signal onto all
501 time-points of the CGaMP recording (Suppl.Fig.1A). If the animal movement was
502 considerable, a 3D drift correction was applied on the GFP signal before merging the two
503 channels. Eventual misalignment between the two signals (caused by drifts or animal
504 movement) was corrected by writing a Fiji/ImageJ macro for manually guided realignment
505 (Suppl.Fig.1B). A final 3D drift correction (89) was then performed for better stabilization.
506 The recording was transferred in Imaris for automatic segmentation with spots of 3,5um
507 diameter. Each uniquely identified neuron though spot detection received an identity and a
508 corresponding fluorescence trace over time (Suppl.Fig.1C). An extra spot was created in

proximity to the organ, serving as background fluorescence to be subtracted from all cell spots. Signal processing and downstream analysis were performed with R (90, 91). Normalization of fluorescence values followed the formula $(F_t\text{-}F0)/F0$, F_t being the intensity at timepoint t and F0 the baseline as average intensity of 10 frames prior stimulation. Response amplitude was calculated as the difference between the peak intensity after stimulation (average of 5 frames near the maximal fluorescence value) and F0. All traces were individually inspected to exclude false positive responses. Responses were considered for further analysis if their amplitude was minimum 20% DF/F0. To calculate taste integration percentages (Fig.2), for each a specific dataset we selected all responding neurons and then determined the fraction of neurons activated by one or by multiple tastants / taste groups per animal. Illustrative lists of responding neurons as well as number of neurons and responses considered for analysis within each test category were assembled in Supplementary File 1. Neurons responding to individual tastants were mapped across organs (Fig.4) by manually assessing their relative position and physiological response. Supplementary File 2 contains he activation or deactivation values with frequencies of response above 20% for mapped neurons and the corresponding Wilcoxon signed rank nonparametric test p-values. Figures were generated in RStudio (92) using "ggplot2", "reshape2" and "scales" packages (93-95) or in GraphPad Prism 7 and adjusted in Adobe Illustrator.

Calcium imaging analysis of *VGlut*-positive cells. For recordings of *VGlut*-Gal4 neurons, analysis was entirely performed in Fiji/ImageJ. Cell segmentation was replaced by setting regions of interest (ROI) around each of the 3 somas and fluorescence intensity over time was extracted after applying a z-projection of the stack recordings. Normalization was performed as above and all taste responses were compared to water response for each neuron. Response values and Mann-Whitney tests of comparisons with control were compiled in Supplementary File 3. Analysis and figures were generated in GraphPad Prism 7.

534

535 **Single-cell chemosensory cell suspension preparation for DisCo.**

536 3rd instar larvae of genotype *nsyb*-Gal4 > UAS-*mcd8:GFP; Or83b:RFP* were collected from
537 food, washed in tap water, PBS, dropped in ethanol and again PBS and dissected in ice-cold
538 PBS in such a manner that only the external chemosensory organs were kept, avoiding to
539 include also the pharyngeal tissue containing internal chemosensory organs. The isolated
540 material was then placed on ice in elastase 1 mg/ml in siliconized 2-ml tubes. After dissecting
541 20-30 larvae (20-25 minutes), the tube sample was placed at room temperature to initiate
542 digestion. After 30 minutes the tissues was washed in PBS+BSA0,05% and dissociated by up-
543 down pipetting for 120 times using siliconized 200p pipette tips. Separated TOG and DOG
544 organs were detected using a fluorescence stereomicroscope and manually picked with a glass
545 micropipette, placed in a final dissociation enzyme mix of Collagenase 1mg/ml + Elastase
546 0,5mg/ml for 10-15 minutes for single cell suspension. The reaction was stopped with PBS +
547 BSA 0,05%. Murine inhibitor was added at each step of the dissociation protocol.

548 **Deterministic co-encapsulation (DisCo) of chemosensory neurons for single cell**
549 **transcriptomics.**

550 Microfluidic chip design, fabrication and device handling are described elsewhere (50).
551 Following organ dissociation, target cell suspension was diluted in the cell loading buffer
552 containing PBS 0.01 % BSA (Sigma B8667), 6% Optiprep (Sigma D1556) and Murine
553 RNase inhibitor (NEB M0314L) in the loading tip connected to the DisCo chip. After bead-
554 cell in droplet co-encapsulation, sample droplets were transferred to a bead collection chip.
555 Subsequently to bead capture, washing, reverse transcription (Thermo Scientific EP0753) and
556 Exonuclease I (NEB M0293L) reactions were performed on-chip (61). Beads containing
557 cDNA were then eluted and cDNA was amplified for 21 cycles using Kapa HiFi Hot start

ready mix (Roche #07958935001). Amplified cDNA was then purified (GC biotech CPCR-0050) for quality assessment with Fragment Analyzer (Agilent). Libraries were then tagmented using in-house Tn5 (96), size selected and purified for sequencing on NextSeq 500 system (Illumina) following recommendations from original Drop-seq protocol (97) (20 bp for read 1 and 50 bp for read2) at sequencing depth above 400.000 reads per cell.

Single-cell data pre-processing and analysis. The data analysis was performed using the Drop-seq tools package (62). After pre-processing, reads were aligned to *Drosophila melanogaster* reference genome (Ensembl version 86) using STAR (version 2.7.0.e) (98). Following the alignment, BAM files were processed using the initial package and read-count matrices were generated.

Downstream analysis was done using the Seurat package (65) version 3.1.2 in RStudio. Individual data sets were loaded and used to create separate normalized and scaled Seurat objects of minimum 400 genes per cell. In order to apply unique cell filters we merged the data and then excluded cells with high gene number and high UMIs as potential doublets and cells with high mitochondrial gene percentage indicating potential apoptotic cells. Due to observed correlation between cells with high gene number (nGene, Suppl.Fig.5B) and cells with high UMIs (nCount, Suppl.Fig.5B), by applying UMI threshold at 50000 we also eliminated cells with more than 4000 genes. Cells with mitochondrial gene percentage under 9% were kept for further analysis (Suppl.Fig.5B). Data was then integrated to circumvent batch effects using Seurat functions *FindIntegrationAnchors* and *IntegrateData*. As we were interested in characterizing neurons, we used the *subset* function to keep only cells expressing *nSyb* or *peb* neuronal markers, excluding eventual surrounding tissue or cuticle cells. On the final dataset of 153 neurons PCA (principal component analysis) computation was followed by UMAP embedding and clustering (Suppl.Fig.5C) was performed at 0.5 resolution.

582 **References**

583

584 1. Gerber B, Stocker RF. The *Drosophila* larva as a model for studying chemosensation
585 and chemosensory learning: a review. Chemical senses. 2007;32(1):65-89.
586 2. El-Keredy A, Schleyer M, Konig C, Ekim A, Gerber B. Behavioural analyses of
587 quinine processing in choice, feeding and learning of larval Drosophila. PLoS One.
588 2012;7(7):e40525.
589 3. Konig C, Schleyer M, Leibiger J, El-Keredy A, Gerber B. Bitter-sweet processing in
590 larval *Drosophila*. Chem Senses. 2014;39(6):489-505.
591 4. Kim H, Choi MS, Kang K, Kwon JY. Behavioral Analysis of Bitter Taste Perception
592 in Drosophila Larvae. Chem Senses. 2016;41(1):85-94.
593 5. Schipanski A, Yarali A, Niewalda T, Gerber B. Behavioral analyses of sugar
594 processing in choice, feeding, and learning in larval Drosophila. Chem Senses.
595 2008;33(6):563-73.
596 6. Croset V, Schleyer M, Arguello JR, Gerber B, Benton R. A molecular and neuronal
597 basis for amino acid sensing in the Drosophila larva. Sci Rep. 2016;6:34871.
598 7. Kudow N, Miura D, Schleyer M, Toshima N, Gerber B, Tanimura T. Preference for
599 and learning of amino acids in larval Drosophila. Biol Open. 2017;6(3):365-9.
600 8. Stocker RF. The organization of the chemosensory system in *Drosophila*
601 *melanogaster*: a review. Cell and tissue research. 1994;275(1):3-26.
602 9. Stocker RF. Design of the larval chemosensory system. Adv Exp Med Biol.
603 2008;628:69-81.
604 10. Chandrashekar J, Hoon MA, Ryba NJ, Zuker CS. The receptors and cells for
605 mammalian taste. Nature. 2006;444(7117):288-94.
606 11. Huang AL, Chen XK, Hoon MA, Chandrashekar J, Guo W, Trankner D, et al. The
607 cells and logic for mammalian sour taste detection. Nature. 2006;442(7105):934-8.
608 12. Yarmolinsky DA, Zuker CS, Ryba NJ. Common sense about taste: from mammals to
609 insects. Cell. 2009;139(2):234-44.
610 13. Barretto RPJ, Gillis-Smith S, Chandrashekar J, Yarmolinsky DA, Schnitzer MJ, Ryba
611 NJP, et al. The neural representation of taste quality at the periphery. Nature.
612 2015;517(7534):373-U511.
613 14. Smith DV, St John SJ. Neural coding of gustatory information. Curr Opin Neurobiol.
614 1999;9(4):427-35.
615 15. Wu A, Dvoryanchikov G, Pereira E, Chaudhari N, Roper SD. Breadth of tuning in
616 taste afferent neurons varies with stimulus strength. Nature Communications. 2015;6.
617 16. Tomchik SM, Berg S, Kim JW, Chaudhari N, Roper SD. Breadth of tuning and taste
618 coding in mammalian taste buds. Journal of Neuroscience. 2007;27(40):10840-8.
619 17. Chaudhari N, Roper SD. The cell biology of taste. J Cell Biol. 2010;190(3):285-96.
620 18. Dahanukar A, Lei YT, Kwon JY, Carlson JR. Two Gr genes underlie sugar reception
621 in Drosophila. Neuron. 2007;56(3):503-16.
622 19. Fujii S, Yavuz A, Slone J, Jagge C, Song X, Amrein H. *Drosophila* Sugar Receptors
623 in Sweet Taste Perception, Olfaction, and Internal Nutrient Sensing. Curr Biol. 2015.

624 20. Thorne N, Chromey C, Bray S, Amrein H. Taste perception and coding in Drosophila.
625 Curr Biol. 2004;14(12):1065-79.
626 21. Liman ER, Zhang YV, Montell C. Peripheral coding of taste. Neuron.
627 2014;81(5):984-1000.
628 22. French A, Ali Agha M, Mitra A, Yanagawa A, Sellier MJ, Marion-Poll F. Drosophila
629 Bitter Taste(s). Front Integr Neurosci. 2015;9:58.
630 23. Zhang YV, Ni J, Montell C. The molecular basis for attractive salt-taste coding in
631 Drosophila. Science. 2013;340(6138):1334-8.
632 24. Hussain A, Zhang M, Ucpunar HK, Svensson T, Quillery E, Gompel N, et al.
633 Ionotropic Chemosensory Receptors Mediate the Taste and Smell of Polyamines. Plos
634 Biology. 2016;14(5).
635 25. Lee MJ, Sung HY, Jo H, Kim HW, Choi MS, Kwon JY, et al. Ionotropic Receptor
636 76b Is Required for Gustatory Aversion to Excessive Na+ in Drosophila. Mol Cells.
637 2017;40(10):787-95.
638 26. Tauber JM, Brown EB, Li Y, Yurgel ME, Masek P, Keene AC. A subset of sweet-
639 sensing neurons identified by IR56d are necessary and sufficient for fatty acid taste. PLoS
640 Genet. 2017;13(11):e1007059.
641 27. Ahn JE, Chen Y, Amrein H. Molecular basis of fatty acid taste in Drosophila. Elife.
642 2017;6.
643 28. Ganguly A, Pang L, Duong VK, Lee A, Schoniger H, Varady E, et al. A Molecular
644 and Cellular Context-Dependent Role for Ir76b in Detection of Amino Acid Taste. Cell Rep.
645 2017;18(3):737-50.
646 29. Sanchez-Alcaniz JA, Silbering AF, Croset V, Zappia G, Sivasubramaniam AK, Abuin
647 L, et al. An expression atlas of variant ionotropic glutamate receptors identifies a molecular
648 basis of carbonation sensing. Nat Commun. 2018;9(1):4252.
649 30. Jaeger AH, Stanley M, Weiss ZF, Musso PY, Chan RC, Zhang H, et al. A complex
650 peripheral code for salt taste in Drosophila. Elife. 2018;7.
651 31. Vosshall LB, Stocker RF. Molecular architecture of smell and taste in *Drosophila*.
652 Annual review of neuroscience. 2007;30:505-33.
653 32. Scott K, Brady R, Jr., Cravchik A, Morozov P, Rzhetsky A, Zuker C, et al. A
654 chemosensory gene family encoding candidate gustatory and olfactory receptors in
655 *Drosophila*. Cell. 2001;104(5):661-73.
656 33. Colomb J, Grillenzoni N, Ramaekers A, Stocker RF. Architecture of the primary taste
657 center of *Drosophila* melanogaster larvae. The Journal of comparative neurology.
658 2007;502(5):834-47.
659 34. Rimal S, Lee Y. The multidimensional ionotropic receptors of Drosophila
660 melanogaster. Insect Mol Biol. 2018;27(1):1-7.
661 35. Stewart S, Koh TW, Ghosh AC, Carlson JR. Candidate ionotropic taste receptors in
662 the *Drosophila* larva. Proc Natl Acad Sci U S A. 2015.
663 36. Alves G, Salle J, Chaudy S, Dupas S, Maniere G. High-NaCl perception in
664 *Drosophila* melanogaster. J Neurosci. 2014;34(33):10884-91.
665 37. Mast JD, De Moraes CM, Alborn HT, Lavis LD, Stern DL. Evolved differences in
666 larval social behavior mediated by novel pheromones. Elife. 2014;3:e04205.

667 38. Xu J, Sornborger AT, Lee JK, Shen P. Drosophila TRPA channel modulates sugar-
668 stimulated neural excitation, avoidance and social response. Nat Neurosci. 2008;11(6):676-
669 82.
670 39. Kwon JY, Dahanukar A, Weiss LA, Carlson JR. Molecular and cellular organization
671 of the taste system in the *Drosophila* larva. The Journal of neuroscience : the official journal
672 of the Society for Neuroscience. 2011;31(43):15300-9.
673 40. Apostolopoulou AA, Rist A, Thum AS. Taste processing in *Drosophila* larvae.
674 frontiers in integrative Neuroscience. 2015;9.
675 41. Python F, Stocker RF. Adult-like complexity of the larval antennal lobe of D.
676 melanogaster despite markedly low numbers of odorant receptor neurons. J Comp Neurol.
677 2002;445(4):374-87.
678 42. Gendre N, Luer K, Friche S, Grillenzoni N, Ramaekers A, Technau GM, et al.
679 Integration of complex larval chemosensory organs into the adult nervous system of
680 *Drosophila*. Development. 2004;131(1):83-92.
681 43. Larsson MC, Domingos AI, Jones WD, Chiappe ME, Amrein H, Vosshall LB. Or83b
682 encodes a broadly expressed odorant receptor essential for *Drosophila* olfaction. Neuron.
683 2004;43(5):703-14.
684 44. Kreher SA, Kwon JY, Carlson JR. The molecular basis of odor coding in the
685 *Drosophila* larva. Neuron. 2005;46(3):445-56.
686 45. Fishilevich E, Domingos AI, Asahina K, Naef F, Vosshall LB, Louis M. Chemotaxis
687 behavior mediated by single larval olfactory neurons in *Drosophila*. Current biology : CB.
688 2005;15(23):2086-96.
689 46. Mathew D, Martelli C, Kelley-Swift E, Brusalis C, Gershow M, Samuel AD, et al.
690 Functional diversity among sensory receptors in a Drosophila olfactory circuit. Proc Natl
691 Acad Sci U S A. 2013;110(23):E2134-43.
692 47. Si G, Kanwal JK, Hu Y, Tabone CJ, Baron J, Berck M, et al. Structured Odorant
693 Response Patterns across a Complete Olfactory Receptor Neuron Population. Neuron.
694 2019;101(5):950-62 e7.
695 48. van Giesen L, Hernandez-Nunez L, Delasoie-Baranek S, Colombo M, Renaud P,
696 Bruggmann R, et al. Multimodal stimulus coding by a gustatory sensory neuron in
697 Drosophila larvae. Nat Commun. 2016;7:10687.
698 49. Rist A, Thum AS. A map of sensilla and neurons in the taste system of drosophila
699 larvae. J Comp Neurol. 2017;525(18):3865-89.
700 50. Bues J, Biočanin M, Pezoldt J, Dainese R, Chrisnandy A, Rezakhani S, et al.
701 Deterministic scRNA-seq of individual intestinal organoids reveals new subtypes and
702 coexisting distinct stem cell pools. BioRxiv. 2020.
703 51. Su CY, Menuz K, Reisert J, Carlson JR. Non-synaptic inhibition between grouped
704 neurons in an olfactory circuit. Nature. 2012;492(7427):66-71.
705 52. Zhang Y, Tsang TK, Bushong EA, Chu LA, Chiang AS, Ellisman MH, et al.
706 Asymmetric ephaptic inhibition between compartmentalized olfactory receptor neurons. Nat
707 Commun. 2019;10(1):1560.
708 53. Python F, Stocker RF. Immunoreactivity against choline acetyltransferase, gamma-
709 aminobutyric acid, histamine, octopamine, and serotonin in the larval chemosensory system
710 of Dosophila melanogaster. J Comp Neurol. 2002;453(2):157-67.

711 54. Brunet Avalos C, Maier GL, Bruggmann R, Sprecher SG. Single cell transcriptome
712 atlas of the Drosophila larval brain. Elife. 2019;8.
713 55. Chen TW, Wardill TJ, Sun Y, Pulver SR, Renninger SL, Baohan A, et al.
714 Ultrasensitive fluorescent proteins for imaging neuronal activity. Nature.
715 2013;499(7458):295-300.
716 56. Egger B, Boone JQ, Stevens NR, Brand AH, Doe CQ. Regulation of spindle
717 orientation and neural stem cell fate in the Drosophila optic lobe. Neural Dev. 2007;2:1.
718 57. van Giesen L, Neagu-Maier GL, Kwon JY, Sprecher SG. A microfluidics-based
719 method for measuring neuronal activity in Drosophila chemosensory neurons. Nat Protoc.
720 2016;11(12):2389-400.
721 58. Marella S, Fischler W, Kong P, Asgarian S, Rueckert E, Scott K. Imaging taste
722 responses in the fly brain reveals a functional map of taste category and behavior. Neuron.
723 2006;49(2):285-95.
724 59. Park J, Carlson JR. Physiological responses of the Drosophila labellum to amino
725 acids. J Neurogenet. 2018;32(1):27-36.
726 60. Faber DS, Pereda AE. Two Forms of Electrical Transmission Between Neurons.
727 Front Mol Neurosci. 2018;11:427.
728 61. Biocanin M, Bues J, Dainese R, Amstad E, Deplancke B. Simplified Drop-seq
729 workflow with minimized bead loss using a bead capture and processing microfluidic chip.
730 Lab Chip. 2019;19(9):1610-20.
731 62. Macosko EZ, Basu A, Satija R, Nemesh J, Shekhar K, Goldman M, et al. Highly
732 Parallel Genome-wide Expression Profiling of Individual Cells Using Nanoliter Droplets.
733 Cell. 2015;161(5):1202-14.
734 63. Klein AM, Macosko E. InDrops and Drop-seq technologies for single-cell
735 sequencing. Lab Chip. 2017;17(15):2540-1.
736 64. Satija R, Farrell JA, Gennert D, Schier AF, Regev A. Spatial reconstruction of single-
737 cell gene expression data. Nat Biotechnol. 2015;33(5):495-502.
738 65. Stuart T, Butler A, Hoffman P, Hafemeister C, Papalexi E, Mauck WM, 3rd, et al.
739 Comprehensive Integration of Single-Cell Data. Cell. 2019;177(7):1888-902 e21.
740 66. Rusch DB, Kaufman TC. Regulation of proboscipedia in Drosophila by homeotic
741 selector genes. Genetics. 2000;156(1):183-94.
742 67. Salvaterra PM, Kitamoto T. Drosophila cholinergic neurons and processes visualized
743 with Gal4/UAS-GFP. Brain Res Gene Expr Patterns. 2001;1(1):73-82.
744 68. Stocker RF. The Organization of the Chemosensory System in Drosophila-
745 Melanogaster - a Review. Cell and Tissue Research. 1994;275(1):3-26.
746 69. Chu-Wang IW, Axtell RC. Fine structure of the terminal organ of the house fly larva,
747 Musca domestica L. Z Zellforsch Mikrosk Anat. 1972;127(3):287-305.
748 70. Jeong YT, Oh SM, Shim J, Seo JT, Kwon JY, Moon SJ. Mechanosensory neurons
749 control sweet sensing in Drosophila. Nat Commun. 2016;7:12872.
750 71. Sanchez-Alcaniz JA, Zappia G, Marion-Poll F, Benton R. A mechanosensory receptor
751 required for food texture detection in Drosophila. Nat Commun. 2017;8:14192.
752 72. Apostolopoulou AA, Hersperger F, Mazija L, Widmann A, Wust A, Thum AS.
753 Composition of agarose substrate affects behavioral output of *Drosophila* larvae. Frontiers in
754 behavioral neuroscience. 2014;8:11.

755 73. Kudow N, Kamikouchi A, Tanimura T. Softness sensing and learning in Drosophila
756 larvae. J Exp Biol. 2019;222(Pt 7).
757 74. Tracey WD, Jr., Wilson RI, Laurent G, Benzer S. painless, a Drosophila gene
758 essential for nociception. Cell. 2003;113(2):261-73.
759 75. Brown TD. Techniques for mechanical stimulation of cells in vitro: a review. J
760 Biomech. 2000;33(1):3-14.
761 76. Reiter S, Campillo Rodriguez C, Sun K, Stopfer M. Spatiotemporal Coding of
762 Individual Chemicals by the Gustatory System. J Neurosci. 2015;35(35):12309-21.
763 77. Hernandez-Nunez L, Belina J, Klein M, Si G, Claus L, Carlson JR, et al. Reverse-
764 correlation analysis of navigation dynamics in larva using optogenetics. Elife. 2015;4.
765 78. Jisoo Han MC. Comprehensive functional screening of taste sensation in vivo.
766 bioRxiv. 2018.
767 79. Smith DV, Travers JB. Metric for the Breadth of Tuning of Gustatory Neurons.
768 Chemical Senses & Flavour. 1979;4(3):215-29.
769 80. Jefferys JG. Nonsynaptic modulation of neuronal activity in the brain: electric
770 currents and extracellular ions. Physiol Rev. 1995;75(4):689-723.
771 81. Miriyala A, Kessler S, Rind FC, Wright GA. Burst Firing in Bee Gustatory Neurons
772 Prevents Adaptation. Curr Biol. 2018;28(10):1585-94 e3.
773 82. Saro G, Lia AS, Thapliyal S, Marques F, Busch KE, Glauser DA. Specific Ion
774 Channels Control Sensory Gain, Sensitivity, and Kinetics in a Tonic Thermonociceptor. Cell
775 Rep. 2020;30(2):397-408 e4.
776 83. Meissner GW, Nern A, Singer RH, Wong AM, Malkesman O, Long X. Mapping
777 Neurotransmitter Identity in the Whole-Mount Drosophila Brain Using Multiplex High-
778 Throughput Fluorescence in Situ Hybridization. Genetics. 2019;211(2):473-82.
779 84. Xu Y, Qin S, Niu Y, Gong T, Zhang Z, Fu Y. Effect of fluid shear stress on the
780 internalization of kidney-targeted delivery systems in renal tubular epithelial cells. Acta
781 Pharm Sin B. 2020;10(4):680-92.
782 85. White CR, Frangos JA. The shear stress of it all: the cell membrane and
783 mechanochemical transduction. Philos Trans R Soc Lond B Biol Sci. 2007;362(1484):1459-
784 67.
785 86. Al-Anzi B, Tracey WD, Jr., Benzer S. Response of Drosophila to wasabi is mediated
786 by painless, the fly homolog of mammalian TRPA1/ANKTM1. Curr Biol. 2006;16(10):1034-
787 40.
788 87. Singh RN, Singh K. Fine-Structure of the Sensory Organs of *Drosophila-*
789 *Melanogaster* Meigen Larva (Diptera, Drosophilidae). International Journal of Insect
790 Morphology & Embryology. 1984;13(4):255-73.
791 88. Schindelin J, Arganda-Carreras I, Frise E, Kaynig V, Longair M, Pietzsch T, et al.
792 Fiji: an open-source platform for biological-image analysis. Nat Methods. 2012;9(7):676-82.
793 89. Parslow A, Cardona A, Bryson-Richardson RJ. Sample drift correction following 4D
794 confocal time-lapse imaging. J Vis Exp. 2014(86).
795 90. Team RC. R: A language and environment for statistical computing. R Foundation for
796 Statistical Computing, Vienna, Austria. URL https://www.R-project.org/. 2017.
797 91. Wickham H. FR, Henry L. and Müller K. dplyr: A Grammar of Data Manipulation. R
798 package version 0.7.6. https://CRAN.R-project.org/package=dplyr. 2018.

799 92. Team R. RStudio: Integrated Development for R. 2015.
800 93. Wickham H. Reshaping Data with the reshape Package. Journal of Statistical
801 Software. 2007;21(12):1-20.
802 94. Wickham H. ggplot2: Elegant Graphics for Data Analysis. 2009.
803 95. Wickham H. SD, RStudio. scales: Scale Functions for Visualization. 2019.
804 96. Picelli S, Bjorklund AK, Reinius B, Sagasser S, Winberg G, Sandberg R. Tn5
805 transposase and tagmentation procedures for massively scaled sequencing projects. Genome
806 Res. 2014;24(12):2033-40.
807 97. Macosko E.Z. GM, McCarroll S.A. Drop-Seq Laboratory Protocol version 3.1. 2015.
808 98. Dobin A, Davis CA, Schlesinger F, Drenkow J, Zaleski C, Jha S, et al. STAR:
809 ultrafast universal RNA-seq aligner. Bioinformatics. 2013;29(1):15-21.

810

Acknowledgements

We thank the Sprecher lab for support and useful discussions and Joern Pezoldt, Wanze Chen and Maria Litovchenko from Deplancke lab for support, valuable comments and practical advice. We thank EPFL's Gene Expression Core Facility for sequencing support and Rommelaere Samuel from Lemaitre lab for providing fluorescent microscope during single-cell preparation experiments. We are also grateful to Boris Egger for guidance on microscopy and data analysis and to everyone who shared with us fly stocks and reagents.

Author contributions

GLM and SGS designed the study and wrote the paper. GLM performed physiological recordings, immunostainings, and single cell dissociation, analyzed the data and created the figures. MB and JB performed DisCo experiments and library preparation. FM wrote the plugins and macros necessary for calcium imaging data processing and assisted in establishing the analysis pipeline. CBA identified and determined *proboscipedia* immunofluorescence expression and assisted with single cell sequencing analysis in Seurat. BD, JYK and SGS assisted in interpretation of results.

Additional information. The authors declare no competing interests.

Funding. This project was supported by the Swiss National Science Foundation (project grant 310030_188471) to SGS.

Data Availability

Single cell RNAseq data reported in this study are available on NCBI GEO; accession number GSE149975.

832 Fiji/ImageJ plugin and macro for calcium imaging data processing are available as
833 supplementary file.

834 Data generated and analyzed within the present study are available from the corresponding
835 author upon request.

836

Figure 1: Peripheral taste neurons of the fruit fly larva – visualization and calcium imaging.

A. The chemosensory system of the larva. External sense organs extend dendrites to the periphery and have main olfactory function – the DOG (dorsal organ ganglion), or gustatory function – the TOG (terminal organ ganglion) and the VOG (ventral organ ganglion). Dendrites of the internal dorsal, ventral and posterior pharyngeal sense organs (DPS, VPS and PPS) innervate the pharynx, thus involved in taste sensing during food ingestion. All chemosensory neurons project axons to the brain in the subesophageal ganglion (SOG) – first central taste integration relay – or to the antennal lobe (AL) for central olfactory processing. Adapted from (1).

B. External chemosensory organs. 7 GSNs previously identified and named C1-C7 are represented here by the color code they were first described with (39, 48). Used Gal4 lines: *Gr22e*-Gal4 (C1), *Gr94a*-Gal4 (C2), *Gr59d*-Gal4 (C1, C2, C4), *Gr66a*-Gal4 (C1, C2, C3, C4), *Gr59e*-Gal4 (C5), *Gr21a*-Gal4 (C6), *GMR57BO4*-Gal4 (C7).

C. UAS-*myrGFP* reporter was expressed in individual GSNs using corresponding Gal4 lines (B). We observed a relatively stereotypic position of specific neurons within the organ across animals ($n \geq 3$) – exemplified on C6 and C1.

D. Illustrative 3D map of TOG segmented cells. Position of neurons with known identities (white dots) is approximated based on separate immunostainings.

E. Representative recording of the larval primary taste organ stimulated with citric acid 100mM. Cytoplasmic expression of *GCaMP6m* and nuclear expression of *RFP* in all neurons (upper left panel) and cell segmentation (white spots, lower left panel). Responding neurons are indicated by blue, red and magenta arrows (upper right panel) and by dots and corresponding fluorescence traces of same colors (lower right panels).

Supplementary Figure 1: Whole organ calcium imaging – data processing.

A. The RFP nuclear signal acquired as a single stack was duplicated to all timepoints of the GCaMP time-series using an in-house written plugin. Step performed in Fiji/ImageJ.
B. On the recording comprising both fluorescence channels, any misalignment between the two signals due to animal movement or slight drift was corrected through a manually assisted macro. Step performed in Fiji/ImageJ.
C. The resulting stabilized and aligned recording was transferred to Imaris for cell segmentation (middle panel) and extraction of corresponding fluorescence traces (right panel). Traces of neurons responding to sucrose 500mM in a representative recording. Steps performed in Imaris and in RStudio.

Supplementary Video 1: Whole organ recording and cell segmentation.

The TOG (larval main peripheral taste organ) recorded using genetically encoded GCaMP reporter in all neurons. The second fluorophore, nuclear RFP, is used for cell segmentation, allowing creation of spots corresponding to each individual neuron. GCaMP fluorescence intensity over time for each spot is represented by spot color, ranging from blue (low signal) to red (high intensity).

Figure 2: Taste neurons show high proportions of taste multimodality and opposed valence integration.

A. GSN responses to series of individual tastants. Illustrative cell responses (y axis) for each tastant series (x axis). Colors were scaled to reflect the intensity of activation to the given taste. Only responses above 20% DF/F were taken into account. Taste stimulation

was done with 5 tastants per animal, each belonging to one of the 5 canonical taste modalities represented along the x axis: sweet (shades of red), bitter (blue), salt (purple), amino acids (brown) and sour (yellow). We used 2 different series of taste recordings. Series 1 consisted of sucrose 500mM for sweet taste, denatonium 10mM for bitter, NaCl 1M for high salt, valine 100mM as amino acid and citric acid 100mM for sour taste; correspondingly, the second series consisted of sucrose 500mM, quinine 5mM, Nacl 100mM for low salt, arginine 100mM and citric acid 100mM. 7 separate organs were recorded within the first series and 8 within the second (N=15). Total percentages of taste integration per neuron per animal are represented on the pie chart: 66% of total responding neurons were activated by only one tastant per organ and up to 34% of neurons responded to more than one tastant. Most unimodal responses (uni-taste / cell, left bar-chart) were recorded to sucrose and to high salt. Conversely, different combinations of taste categories were observed to activate single neurons, with different frequency of occurrence (multi-taste / cell, right bar-chart). The most frequent combinations of taste modalities per cell per animal were sweet + amino acid, sweet + sour, sour + high salt, sweet + high salt and sweet + bitter. Some of these combinations involve a presumed positive valence (sucrose/sweet) taste together with a negative valence taste (bitter or high salt) sensed by the same neuron.

B. Stimulation with groups of tastants comprising 2 sugar categories (mono and disaccharides), low and high salt concentration, 4 amino acid and 2 bitter groups. Responses of above 20% DF/F intensity threshold were considered.

Upper panels: Among all neurons responding to sugar group stimulation, we observed a comparable ratio of cells activated by only one sugar category and 25.4% activated by both mono and disaccharides. For salt-responding neurons, a higher proportion showed unique activation to high salt than to low salt concentration, and 20% neurons responded

to both categories. Amino acids split in 4 groups gave a rounded 62% to 38% ratio of uni- to multi-group response integration, calculated among all amino acid-responding neurons. Taking into account total responding neurons from animals stimulated with all 8 groups resulted in 60% to 40% uni- to multi-modality group response integration.

Lower panels: Within the total number of bitter-responsive neurons, 55% were uniquely activated by stimulation with DSoTC group and respectively 30% by QLSC group. Integration between sweet and bitter taste has been calculated on responding neurons from animals stimulated with 2 groups of each modality: we observed similar proportions of taste cells responding only to bitter groups (30,3%), cells responding only to sugar (39,4%) and cells responding to groups from both modalities (30,3%).

Figure 3: GSNs can respond to taste through activation or deactivation.

A. Illustration of a segmented TOG with two highlighted neighboring neurons (white dots) called CDL1, labeled in red and corresponding red fluorescence traces, and CDL2 with corresponding blue traces. When stimulated with citric acid 100mM CDL1 generally responds with a canonical activation of fluorescence intensity increase, while the adjacent CDL2 responds with a simultaneous deactivation, or a fluorescence intensity decrease.
B. Cutting connections between chemosensory organs and brain (left panel illustration) did not abolish the synchronous activation-deactivation response to citric acid stimulation observed in CDL1-CDL2 neuronal couple (right panel).

Figure 4: Mapping neuronal responses shows a high level of taste multimodality.

A. Manual matching of responding GSNs across recorded organs (N=15) stimulated with series of individual tastants (Fig.2A). 21 neuronal identities displayed on the y-axis. The total response frequency (freq) of each neuron is represented in shades of grey (darker for higher frequency) and translates how often the given neuron has been recorded to respond above 20% DF/F0. For each mapped neuron the activation (yellow-red colors) and deactivation (light-dark blue colors) to a respective tastant is displayed as heatmap for both frequency and amplitude of response. Frequency of response (ovals) shows how consistently a mapped neuron responded to a particular tastant. Response amplitudes (squares) were plotted only for frequencies above 20% (N≥3), scaled and reflected by color intensity of squares. To ease overall interpretation, denatonium and quinine were grouped under the label "bitter", and valine and arginine as "amino acid".

B. 3D representative visualization of matched neurons.

C. CDL1 is activated by sucrose, citric acid and high salt, responding most robustly (most frequently) to citric acid (red square, upper panel). By contrast, CDL2 is activated by sucrose and denatonium, eliciting fluorescence deactivation to sucrose, low salt and most frequently to citric acid (red square, lower panel).

D. AC1 is potentially the previously characterized C6 based on the very particular anterior position in the organ (as shown in Fig.1C) and on detected responses to sucrose and high salt, as previously described (48).

Figure 5: Single-cell RNA sequencing of chemosensory neurons.

A. Single cell dissociation protocol; manual picking of the fluorescently labelled sense organs. For chemosensory organ identification, green fluorescence can be driven in all neurons by a pan-neuronal driver line or in a subpopulation as labeled by *Ir76b*. *RFP* as a tag to *Orco*, olfactory co-receptor present in olfactory cells, labels only DOG.

B. Integrated data sets as a single object in Seurat, represented in an UMAP embedding. The final dataset after processing contains 153 cells expressing neuronal markers such as *Neuroglian (Nrg), Synaptobrevin (Syb)*, *neuronal Synaptobrevin (nSyb)* or *pebbled (peb)*.

C. *Odorant receptor co-receptor* (*Orco)* is expressed in the DOG and *proboscipedia (pb)* in the TOG. Their molecular expression appears largely non-overlapping in single cells. Immunostainings against the RFP-tagged *Orco* showed expression restricted to the DOG, as expected; *pb* expression shown by anti-Pb staining at embryonic stage labels TOG but not DOG neurons.

Supplementary Figure 5: Single-cell RNA sequencing of chemosensory neurons.

A. Schematic principle of DisCo (DeterminIStic CO-encapsulation) with optimized co-encapsulation efficiency for minimal cell loss. DropSeq on a microfluidic chip equipped with valves that allow single cells (arrow in a.) to be stalled in a designated region (bottom square, b.) until a corresponding barcoded bead (arrow in b.) reaches a second designated region (upper square, c.) for their concomitant release into an oil droplet (d.).

B. Three data sets as biological and technical replicates were merged and filtered to eliminate cells with high gene number (nGene) or high UMIs (nCount) as potential indicator of doublets and cells with high mitochondrial gene expression as indicator of apoptotic cells. Correlation between high gene number and high UMIs (nGene vs nCount) was used for establishing filter thresholds. Integrated data was subset for neurons, resulting in a dataset of 153 cells above 400 genes per cell.

C. UMAP embedding in Seurat was colored by cell cluster association of cells. Neuronal marker *Syb* shows expression in both cell clusters, while *Orco* and *pb* show distinct expression roughly corresponding to the identified clusters.

Figure 6: Neurotransmitters of chemosensory neurons show broad or narrow expression.

A. *Choline acetyltransferase* (*ChAT*/*Cha*) labels all chemosensory neurons using a *Cha*-Gal4 driver (67) (left panels). Corresponding expression in UMAP embedding colored by expression (right panel). Scale bar, 10 µm.

B. *TH* or *pale* (*ple*) is a tyrosine hydroxylase on the dopamine synthesis pathway, expressed in 2 TOG neurons as shown by anti-TH antibody staining (left panels). Corresponding *ple* molecular expression (right panel). Scale bar, 10 µm.

C. *Vesicular glutamate transporter* (*VGlut*) shows restricted expression in 3 neurons, using a *VGlut*-Gal4 line (left panels). *VGlut* narrow expression reflected in the UMAP embedding (right panel). Scale bar, 10 µm.

D. Physiological responses of the 3 *VGlut* expressing cells stimulated with water as control and with eight tastants introduced earlier (Fig.2A & 4). Mann-Whitney statistical test was used for comparisons between responses to water and each tastant (Suppl.File3): TOG neuron (left panel) responded to sucrose and to valine; Mec (neuron localized anterior-laterally to TOG, middle panel) showed no responses distinct from water; DOG neuron (right panel) responded to sucrose. Data presented as mean + SEM (error bars) and dots represent individual responses from separate experiments.

Supplementary Figure 6: *VGlut*-expressing TOG neuron does not co-localize with C2 or with C7.

VGlut-positive TOG neuron (**A.**) does not share identity with C2 (**B.**), C7 (**C.**) or C1 (**D.**), using corresponding Gal4 lines and comparing the number of GFP positive cells in separate versus crossed lines. Scale bars, 10 µm.

Figure 7: Co-expression of neurotransmitter markers.

A. *DAT* and *Vmat* share expression in single cells (magenta dots, blue arrows), as transporters of dopamine and respectively monoamines, the later inclusive of the first.

B. Double cholinergic and dopaminergic profile as illustrated by a few cells (blue arrows).

C. Co-expression of GABAergic *GABA-B-R2* and serotonergic *5-HT2B* receptors.

D. Neuropeptide *Nplp4* present in a few *VGlut*-positive cells.

E. Neuropeptide *Nplp2* co-localizes with *Vmat* (blue arrows).

Figure 8: Chemosensory neurons express mechanosensory markers.

A. *nan*-Gal4 labels 1 TOG and 1 DOG neuron (left panel), scarce expression mirrored by the UMAP embedding colored by expression (right panel). Scale bar, 10 µm.

B. *nompC*-Gal4 has been identified in 3 chemosensory cells (left panel), paralleled by UMAP embedding (right panel). Scale bar, 10 µm.

C. *pain*-Gal4 labels a larger subpopulation of TOG neurons. We recorded neuronal response of *pain*-expressing neurons pre-exposed to water: mechanical stimulation produced by water pump switch ON/OFF. Responding cells in a 3D representation and respective fluorescence traces. Representative traces for 3 cells, each from two different animals.

Supplementary Figure 8: Response to both gustatory and mechanical stimulation in a TOG neuron.

CM1 cell identified in a pan-neuronal whole-organ recording responds to sucrose 500mM and is deactivated when the water flow pump is turned on. The cell was already exposed

to water inside the microfluidic channel, and therefore the response is likely not determined by water itself but by shear stress on the cell membrane.

Supplementary Table 1. Chemicals used for taste stimulation.

Supplementary File 1. Data referring to Fig.2.

Supplementary File 2. Data referring to Fig.4.

Supplementary File 3. Data referring to Fig.6C.

Supplementary File 4. Whole organ calcium imaging, data processing, Suppl.Fig1 – ImageJ scripts and pipeline instruction files.

Figure 1: Individual neurons of the TOG

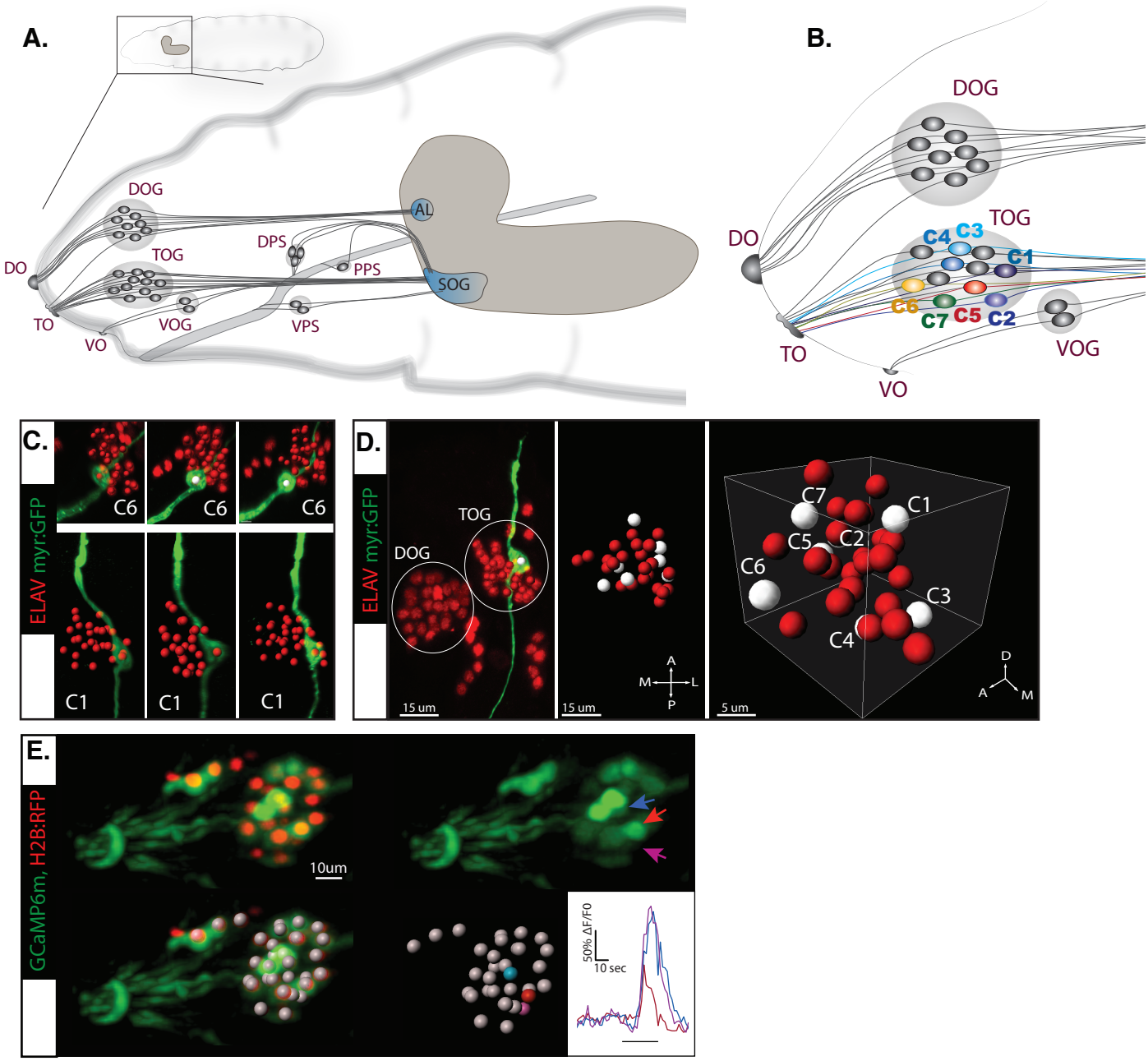

Supplementary Figure 1: Whole-organ recording -data processing.

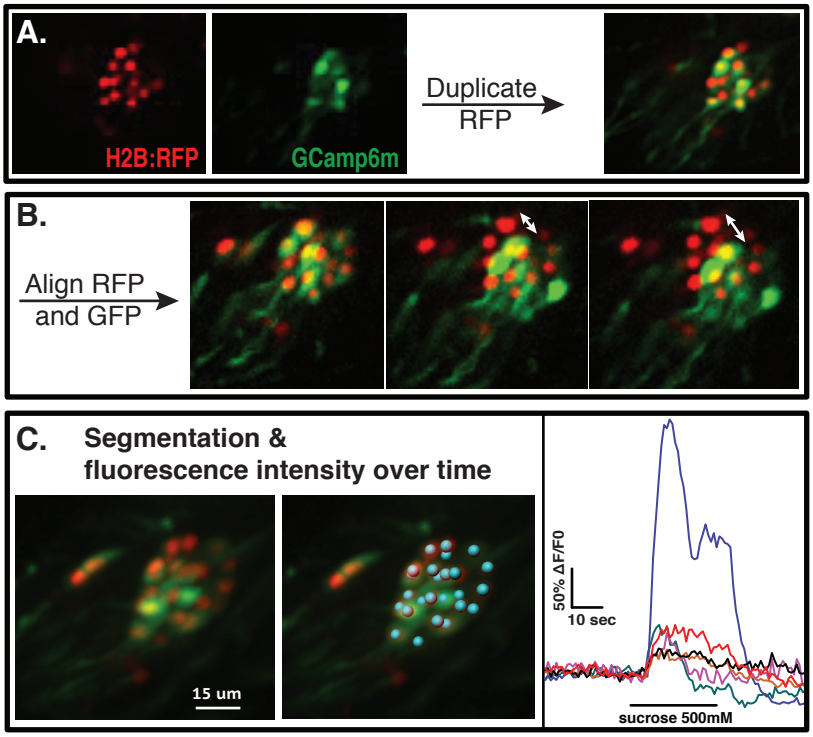

Figure 2: Tunning of response.

A. GSN responses to series of individual tastants.

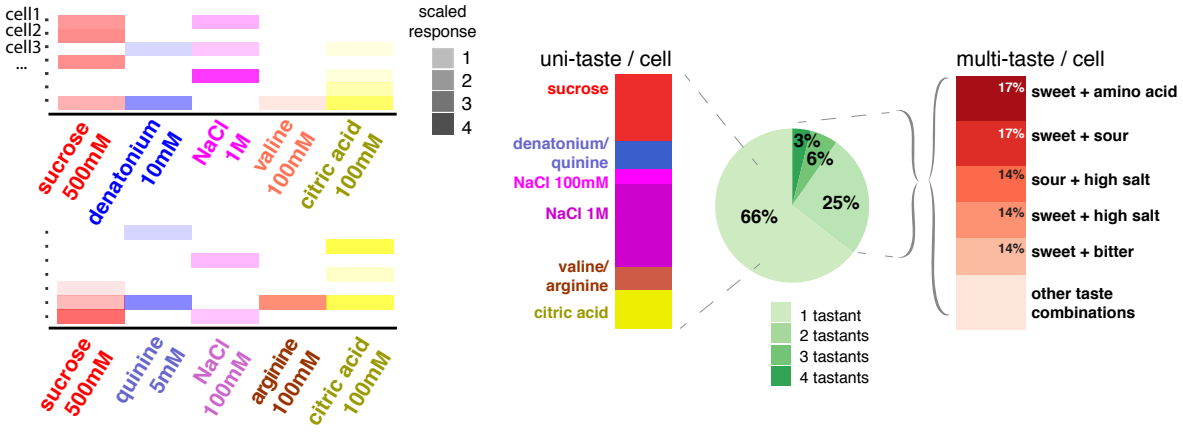

B. GSN responses to taste groups.

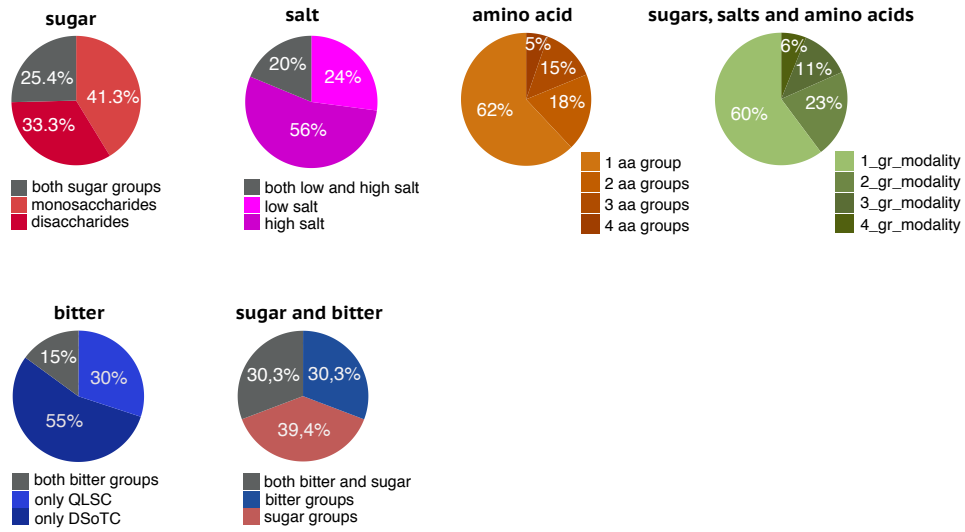

Figure 3: Activation and deactivation responses in taste neurons.

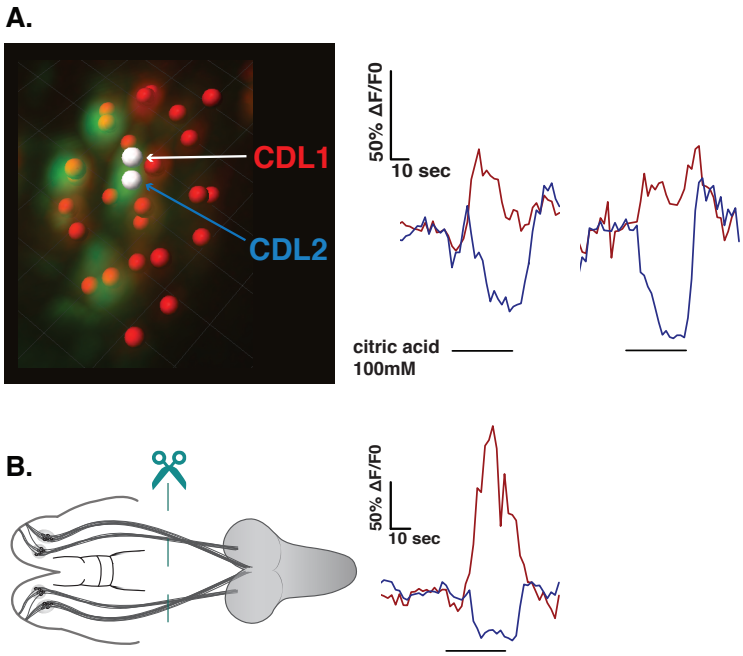

Figure 4: Map of intensity and frequency of response.

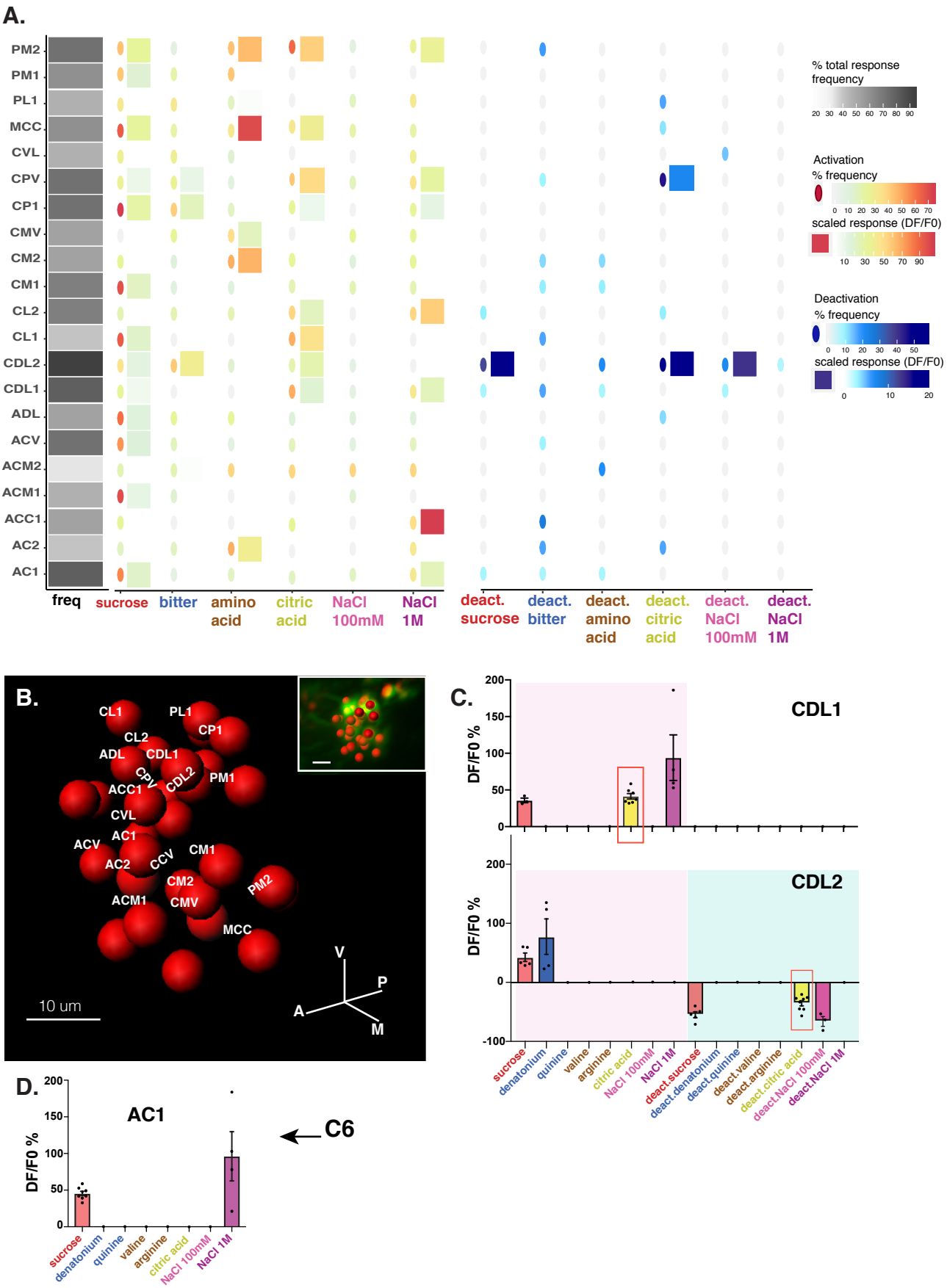

Figure 5: Single cell RNA sequencing of chemosensory neurons.

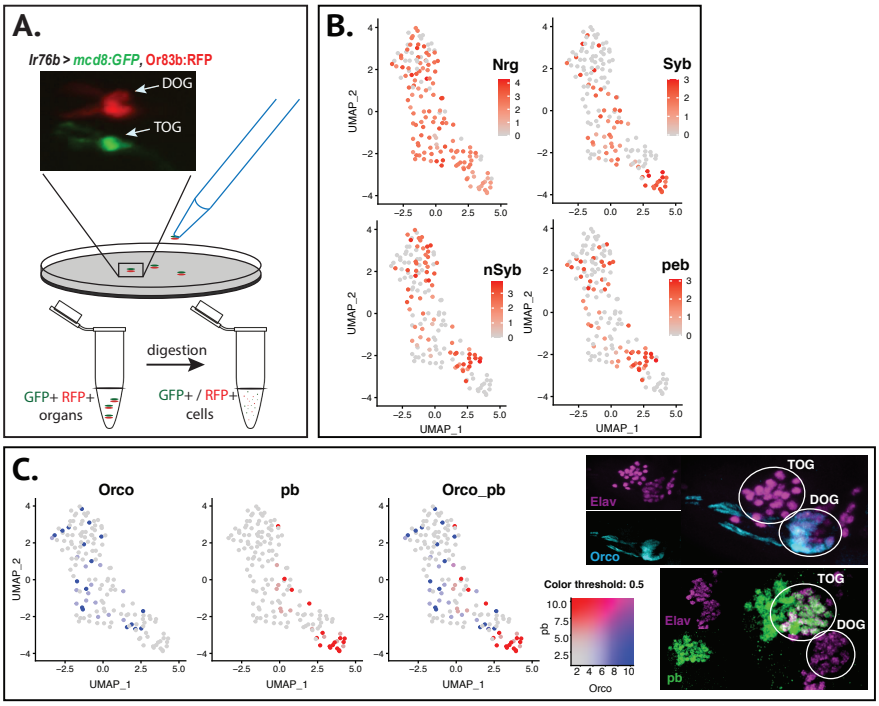

Supplementary Figure 5: Single cell RNA sequencing of chemosensory neurons.

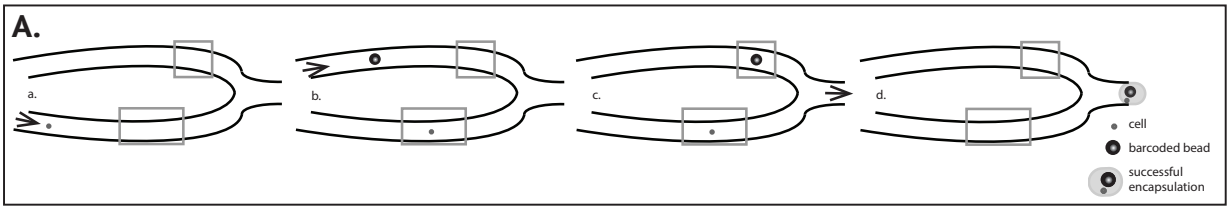

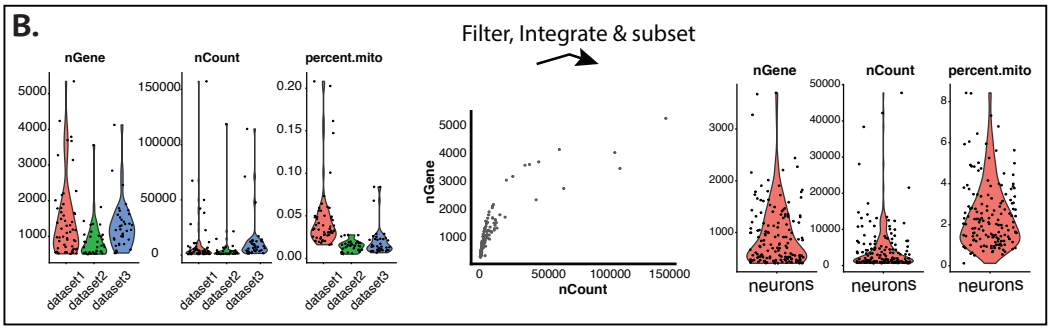

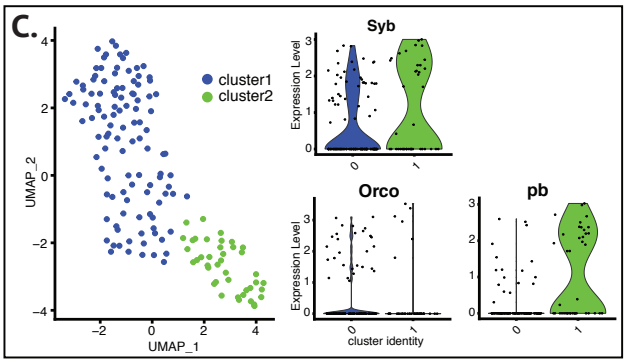

Figure 6: Neurotransmitters of chemosensory neurons show broad or narrow expression

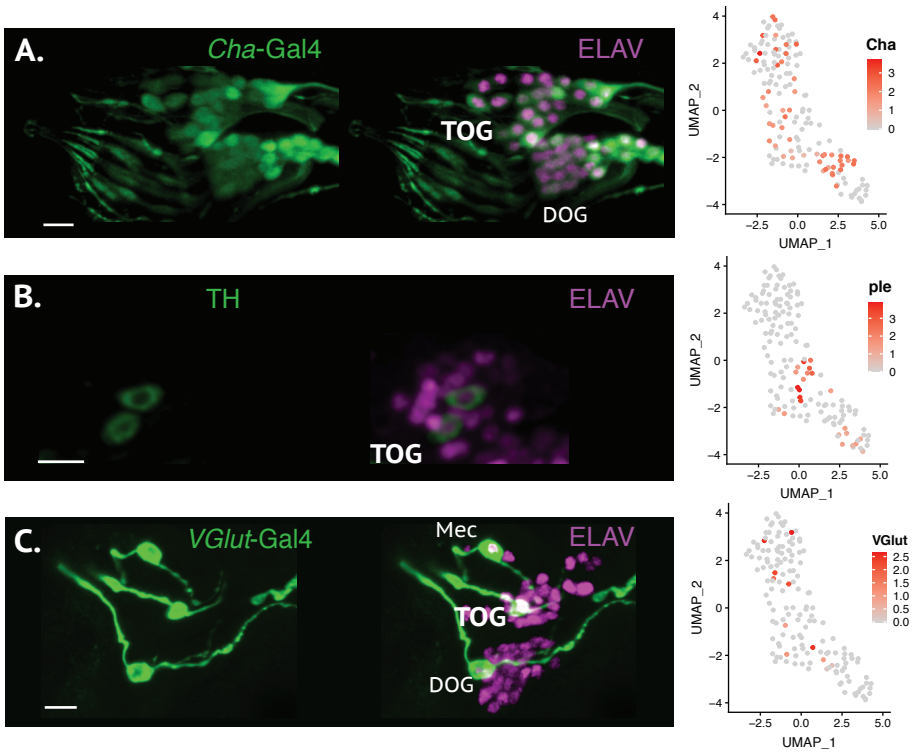

D. ***VGlut*-Gal4 > UAS-*GCaMP6m***

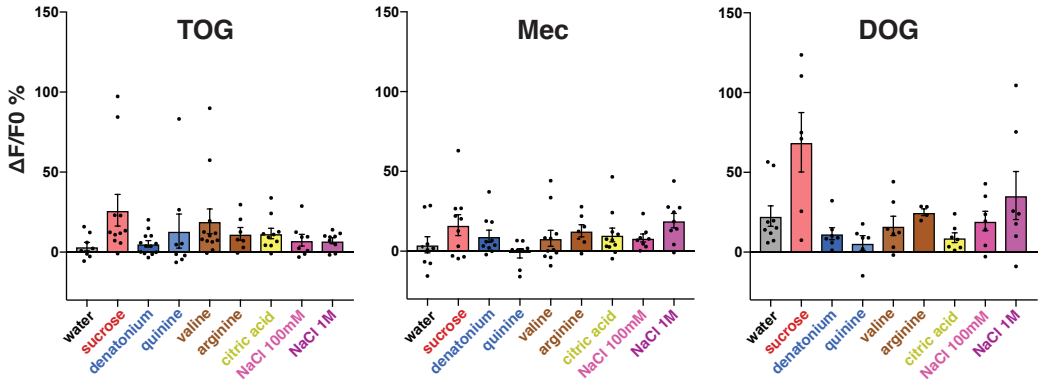

Supplementary Figure 6: *VGlut*-positive TOG neuron doesn't share identity with C2, C7 or C1 neurons.

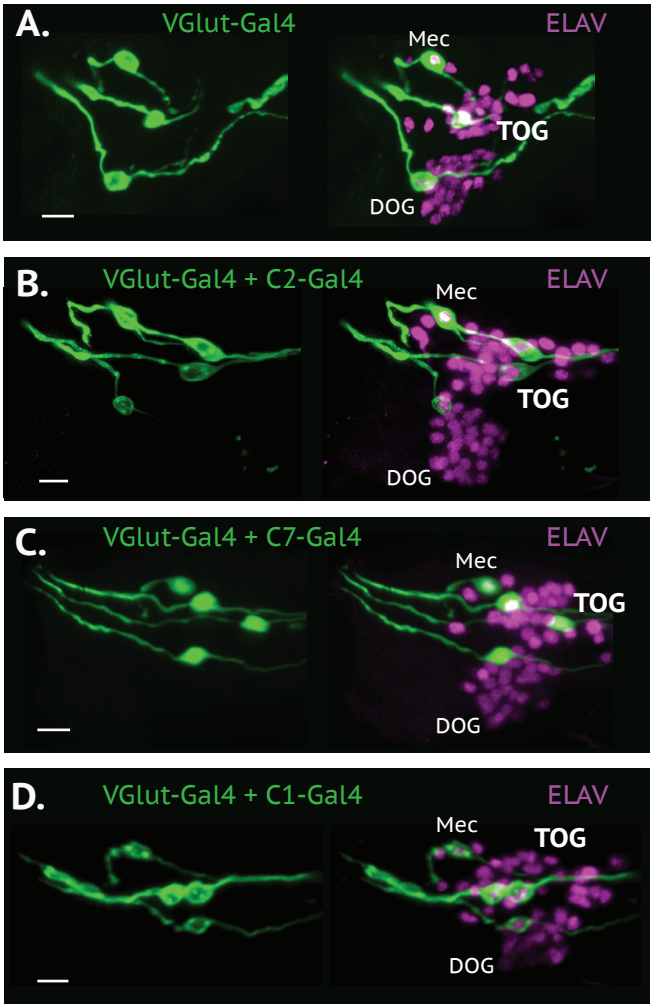

Figure 7: Co-expression of neurotransmitter marker genes.

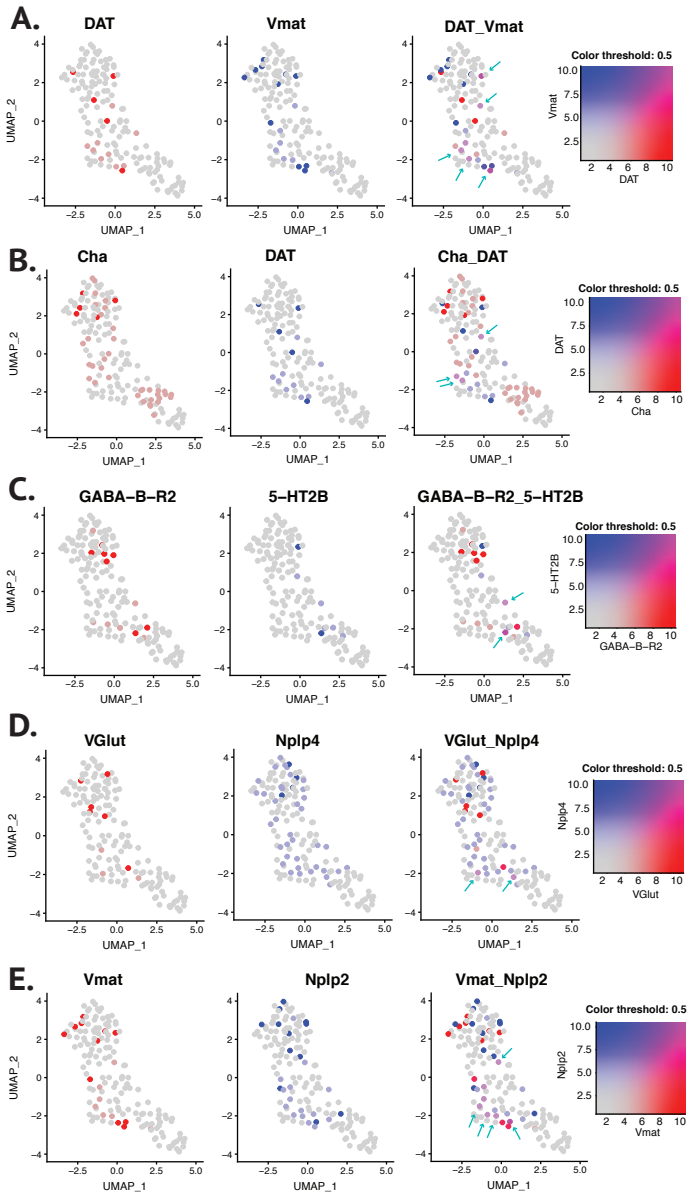

Figure 8: Chemosensory neurons express mechanosensory markers

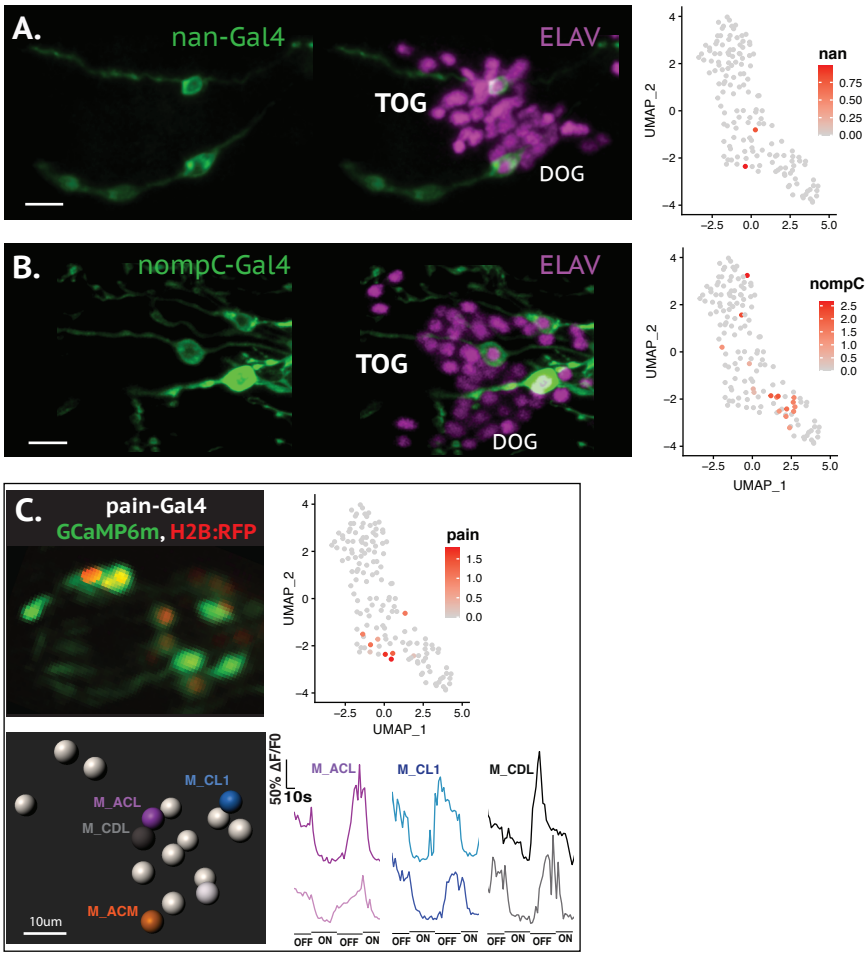

Supplementary Figure 8: Response to both gustatory and mechanical stimulation in a TOG neuron.